The University of Manchester

The University of Manchester Research

Modelling wave attenuation by saltmarsh using satellite-derived vegetation properties

DOI:
10.1016/j.ecoleng.2021.106528

Document Version
Accepted author manuscript

Link to publication record in Manchester Research Explorer

Citation for published version (APA):
Figueroa-Alfaro, R. W., van Rooijen, A., Garzon, J. L., Evans, M., & Harris, A. (2022). Modelling wave attenuation by saltmarsh using satellite-derived vegetation properties. *Ecological Engineering*, *176*, Article 106528. https://doi.org/10.1016/j.ecoleng.2021.106528

Published in:
Ecological Engineering

Citing this paper
Please note that where the full-text provided on Manchester Research Explorer is the Author Accepted Manuscript or Proof version this may differ from the final Published version. If citing, it is advised that you check and use the publisher's definitive version.

General rights
Copyright and moral rights for the publications made accessible in the Research Explorer are retained by the authors and/or other copyright owners and it is a condition of accessing publications that users recognise and abide by the legal requirements associated with these rights.

Takedown policy
If you believe that this document breaches copyright please refer to the University of Manchester’s Takedown Procedures [http://man.ac.uk/04Y6Bo] or contact uml.scholarlycommunications@manchester.ac.uk providing relevant details, so we can investigate your claim.

OPEN ACCESS

Download date:28. Apr. 2024

Modelling wave attenuation by saltmarsh using satellite-derived vegetation properties

Richard W. Figueroa-Alfaro [a,*], Arnold van Rooijen [b], Juan L. Garzon [c], Martin Evans [a], and Angela Harris [a]

[a] *School of Environment, Education and Development, The University of Manchester, M13 9PL, Manchester, United Kingdom*
[b] *Oceans Graduate School and UWA Oceans Institute, University of Western Australia, Crawley, 6009 WA, Australia*
[c] *CIMA – Centre for Marine and Environmental Research, FCT, Universidade do Algarve, Campus de Gambelas, 8005-139 Faro, Portugal*

* Corresponding author. School of Environment, Education and Development, The University of Manchester, M13 9PL, Manchester, United Kingdom
E-mail address: richardwagner1086@gmail.com (R. Figueroa-Alfaro)

Abstract

Saltmarshes are increasingly recognised an important asset in coastal management as they dissipate wave energy and thus reduce the potential for coastal flooding. The frontal surface area (FSA) and the drag coefficient (C_d) are parameters commonly used in wave attenuation models to express the resistance of vegetation structure to incident waves. The FSA of vegetation represents the vertical surface area facing incoming waves which is calculated as the product of height, diameter and density whereas C_d is often used as tunable parameter that represents the vegetation-wave interactions that relies on both vegetation properties and wave conditions. Despite their importance in numerical modelling, substantial uncertainty remains in obtaining these parameters in the field due to the time-intensive and relatively expensive nature of data collection. An alternative structural vegetation parameter that can be included in wave attenuation models is the leaf area index (LAI). The primary advantage of the LAI is that it can be readily derived from satellite imagery, and thus provides a low-cost, fast alternative to field data collection. However, to date, its incorporation in widely-used coastal engineering models is lacking. The aim of this paper is to verify the use of remote-sensed LAI in numerical wave models as an alternative to FSA. Here, the widely used XBeach model for simulating storm impacts on a range of coastal systems is applied to two open coast sites with extensive saltmarsh; Chesapeake Bay, USA, and Brancaster, UK. To assess the performance of wave attenuation modelling using both methods, we compared the use of remote-sensed LAI from satellite imagery and field-based FSA as inputs into the model. The LAI-based model provides similar levels of accuracy as the FSA-based model. Likewise, higher uncertainties related to plant height, diameter, and density were found in the FSA-based model than in the LAI-based model. Therefore, the LAI-based model provides the advantage of a low-cost and fast method to accurately estimate and predict wave attenuation by vegetation using numerical models such as XBeach. Our practical application in the Brancaster site exemplifies an easy and

fast approach to obtaining structural parameters of saltmarsh vegetation and estimating wave attenuation between natural and artificial saltmarshes as well as between seasons.

Keywords: numerical modelling, leaf area index (LAI), remote sensing, wave-vegetation interaction, wave dissipation.

1. Introduction

Saltmarshes are vegetated ecosystems commonly composed of mud or fine sand (Adnitt *et al.*, 2007) and typically located in estuaries, bays, or low-energy intertidal zones (e.g. Leonardi *et al.*, 2018). Saltmarshes may preserve coastlines during sea-level rise due to dynamic equilibrium of sediment accretion by tides (Shepard, *et al.*, 2011) and erosion process due to waves (Gedan *et al.*, 2011). These ecosystems can reduce the peak of the flood (e.g. Glass *et al.*, 2018), provide storm wave energy dissipation (e.g. Bridges *et al.*, 2015), and decrease flow velocities (Schepers *et al.*, 2018). Consequently, saltmarshes are increasingly considered a valuable component in flood protection schemes (Adnitt *et al.*, 2007; Williams *et al.*, 2012; Sutton-Grier *et al.*, 2015) for coastal management. One of the key management questions is whether saltmarsh vegetation provide substantial levels of coastal flood protection, which is one of the motivations for this study.

The wave attenuation capacity of saltmarshes depends on the species present, biomass, plant growth period, and the hydrodynamic conditions (Yang *et al.*, 2012; Garzon *et al.*, 2019b). Specifically, the vegetation structure of saltmarshes has an effect not only on wind-generated sea-swell waves but also on low-frequency infra-gravity (IG) waves and the increase in nearshore mean water level due to wave breaking known as wave setup (van Rooijen *et al.*, 2016). IG waves, with a typical period of 25-250 seconds, are substantial contributors to wave run-up (Stockdon *et al.*, 2006) and generally dissipate across relatively long distances (Phan *et al.*, 2015). Wave setup can account for the

10%–15% of the observed peak surge elevation inside large estuaries (e.g. the Chesapeake Bay) during high energy events (Sheng *et al.*, 2010).

The impact of vegetation structure on wave attenuation is driven by the plant surface area facing the incoming waves (Mendez and Losada, 2004) which is characterised by three biophysical components of vegetation: plant height (h_v), diameter (b_v), and the number of plants per unit area (density, N_v) (e.g. de Vries *et al.*, 2018). A single important parameter derived from the product of these three components is the frontal surface area (FSA = h_v x b_v x N_v) that determines the rate of wave energy attenuation (Shafer and Yozzo, 1998; Suzuki *et al.*, 2012; Marsooli *et al.*, 2016; Marsooli *et al.*, 2017). One relevant dimensionless parameter is the stem-submergence ratio (h_v /h) that relates the plant height to the water depth and significantly impacts wave energy dissipation (Maza *et al.*, 2015; Garzon *et al.*, 2019a). A number of laboratory-based wave attenuation studies have reported clear relationships between FSA and rates of wave energy attenuation, where a larger frontal area results in more dissipation (Smith and Anderson, 2011; Ozeren *et al.*, 2014; Maza *et al.*, 2015). However, the availability of measured FSA through vegetation surveys is limited and requires costly and laborious effort, especially in large areas with constricted access as commonly in the case for saltmarshes. Likewise, FSA may be highly variable both in space and time.

In wave attenuation modelling, another physical parameter to represent vegetation-wave interactions, that mostly include unresolved processes, is the drag coefficient (C_d) which in turn, also affects the rate of wave energy dissipation. Although values for FSA can be obtained in a rather straightforward way due to its direct link to physical properties (e.g. plant height, diameter, and density), this is not the case for the drag coefficient. C_d can vary with several orders of magnitude depending on the hydrodynamic conditions, the plant characteristics (including rigidity), and the method used (e.g., derived from wave height measurements or from direct force observations). It may also be tuned to account for processes that are not accounted in the model (e.g., vegetation flexibility, spatial non-uniformity, array blockage, and sheltering effects). For predictive purposes, previous studies have proposed empirical equations for saltmarsh vegetation describing C_d as a function of the Reynolds number (*Re*) or the Keulegan-Carpenter number (*KC*) (e.g. Mendez and Losada, 2004; Pinsky *et al.*, 2013; Garzon *et al.*, 2019a). Nevertheless, because of all the uncertainties surrounding the drag coefficient and its substantial effect on wave prediction, selecting the best empirical equations for a given field site and wave condition is challenging, hence using constant C_d values obtained from the literature or through model calibration (if wave data is available) is still a common practice (e.g. van Rooijen *et al.*, 2016).

As an alternative to the FSA parameterisation, the frontal area index is a key plant parameter that represents the submerged frontal plant area facing waves. The frontal area index is expressed as the plant frontal area of roughness elements per unit ground area calculated as the product of breadth/width, height and number of plants per unit bed area (Jasinski and Crago, 1999) which is equivalent to FSA. Derived from the frontal area index, the more widely used leaf area index (LAI) defined as the one-sided leaf area per unit ground surface area (Green *et al.*, 1997; Jensen *et al.*, 2002; Bréda, 2003; Jonckheere *et al.*, 2004; Davi *et al.*, 2006; Delegido *et al.*, 2015; Orlando *et al.*, 2016; Korhonen *et al.*, 2017; Casa, Upreti and Pelosi, 2019) can similarly provide information on vegetation vertical structure (Delegido *et al.*, 2011; Clevers *et al.*, 2017). Previous studies have demonstrated that LAI can be a robust parameter to estimate vegetation resistance by describing the impact of leaf mass on vegetative drag (Jalonen *et al.*, 2013) and thus on unidirectional flow resistance (Aberle and Järvelä, 2013). However, these studies have only focused on the relationship between LAI and the consequent vegetation related drag force in unidirectional flows (Tempest *et al.*, 2015) while the direct application of LAI to wave attenuation models has been limited (de Vries *et al.*, 2018).

One of the main advantages of the LAI is that it can be measured using remote sensing technology (Zheng and Moskal, 2009) and thus offers a low-cost, rapid alternative to field survey. In practice, remote sensing can infer LAI measurements that represent the vegetation. For example, Sentinel-2 satellite imagery can be used to derive LAI based on a neural network method (Verrelst *et al.*, 2015; Upreti *et al.*, 2019) with high spatial (10 m) and temporal resolutions (ESA, 2015). This paper aims: (i) to assess how satellite LAI estimations compare to conventional field-derived (FSA) observations of the saltmarsh vegetation structure and (ii) to quantify the uncertainty associated with using FSA in relation to LAI to characterise vegetation structure and its influence on wave attenuation prediction. Specifically, using in situ wave height data from a storm event in the Chesapeake Bay (USA) (Garzon *et al.*, 2019b), we determined the relative sensitivity of wave height attenuation model predictions using FSA and LAI. We subsequently used LAI to model seasonal wave attenuation at a natural and an artificial saltmarsh restoration in Brancaster (UK) to investigate the suitability of the LAI-based model in a real case as a demonstration of the efficacy of this modelling approach for coastal management applications.

2. Materials and methods

In this study, we use satellite data derived from Sentinel-2 MSI imagery as an input to represent vegetation structure for XBeach. The model is parameterised based on the field-based FSA and the remotely-sensed LAI. After that, the model is applied to the Chesapeake Bay, US and Brancaster, UK study sites respectively. In the following sections, the methods are explained in more detail as well as their application.

2.1. Satellite-derived saltmarsh cover

Sentinel-2 is a European wide-swath, high temporal (5-10 days) and spatial (10-60 m) resolution, multispectral imaging mission covering between latitudes 56º south and 84º north that possess a Multi-Spectral Instrument (MSI) payload sensor (ESA, 2015). The MSI dataset consists of spectral information from 13 bands ranging from visible (VIS) to near-infrared (NIR) to shortwave infrared (SWIR) spanning three spatial resolutions (10 m, 20 m and 60 m, respectively). Sentinel-2 MSI surface reflectance imagery was obtained from the Copernicus Open Access Hub (ESA, 2021). To avoid erroneous values of surface reflectance, we manually selected the images where the field site was cloud-free. All spectral bands were subsequently resampled to 10 m spatial resolution (ESA, 2015) and LAI estimates were retrieved using the thematic land processing tool available within the open-source Sentinel Application Platform (SNAP) (Verrelst *et al.*, 2015; Weiss and Baret, 2016; Upreti *et al.*, 2019). We used Sentinel-2 imagery to derive remote-sensed LAI for the Chesapeake Bay, US site on September 10th, 2015 and for Brancaster, UK site on July 23th, 2019 and January 29th, 2020.

2.2. XBeach model description

We used the XBeach model (version 1.23.5426M, Roelvink *et al.*, 2009) to estimate wave attenuation by vegetation. The model includes a vegetation routine (XBeach-Veg) that accounts for the vegetation structure and its effect on the wave and flow damping (van Rooijen *et al.*, 2015, 2016). XBeach has three model options: the stationary wave mode which solves wave-averaged equations; the surf-beat mode that solves short wave energy variation on the scale of wave groups as well as infra-gravity (IG) waves; and the non-hydrostatic mode that fully resolves sea-swell waves and IG waves (Roelvink *et al.*, 2015). Non-linear wave attenuation models can simulate wave dissipation due to vegetation (Ma *et al.*, 2013) using the geometric properties of the canopy (Karambas *et al.*, 2015) and non-linear shallow water equations for infra-gravity waves (van Rooijen *et al.*, 2015).

Here, the surf-beat mode, which is specifically developed for simulating storm impact, was used in one-dimensional (1D) and two-dimensional (2D) mode to estimate wave attenuation. For our simulations, the vegetation characteristics were either based on field-based FSA measurements or remotely-sensed LAI estimates, as discussed in the next section. For all other model settings, default values (Roelvink *et al.*, 2015) were used. Finally, we evaluated the capacity of saltmarshes to attenuate wave energy in terms of sea-swell wave height, IG wave heights, and wave setup.

2.2.1. Model parameterisation using frontal surface area (FSA)

The conventional practice of parameterising wave attenuation by vegetation utilises measurements of plant height (h_v), diameter or blade width (b_v), and the number of plants per area (density, N_v) that could be either from field measurements, expert judgement (estimates) or the literature. The drag coefficient (C_d) is also needed which is challenging to estimate, therefore, this model utilises C_d from empirical formulations from the literature. The XBeach vegetation module in surfbeat mode uses the formulation from Mendez and Losada (2004) for sea-swell wave energy attenuation by vegetation, which was adjusted to consider vertically heterogeneous vegetation similar to Suzuki *et al.* (2012):

$$\varepsilon_v = \frac{1}{2\sqrt{\pi}} \rho C_d \boldsymbol{b_v N_v} \left(\frac{kg}{2\sigma} \right)^3 \frac{\sin h^3 (k\boldsymbol{h_v}) + 3 \sin h(k\boldsymbol{h_v})}{3k \cos h^3 (kh)} {H_{rms}}^3 \qquad (1)$$

where, ε_v = time-averaged vegetation-induced rate of energy dissipation per unit horizontal area, ρ = water density (kg/m^3), C_d = drag coefficient, b_v = vegetation stem diameter (m), N_v = vegetation density (stems/m^2), k = wave number (2π/L); L = wavelength (m), g = gravitational acceleration (m/s^2), σ = wave frequency (rad/sec), h = water depth (m), h_v = vegetation height (m), and H_{rms} = root mean square wave height (m). In this implementation, C_d can be obtained from empirical expressions found in the literature or considered a calibration parameter if wave observations are available.

Garzon *et al.* (2019b) expanded on this FSA-based model by adding several empirical formulations found in the literature, considering simulated and real *Spartina Alterniflora* vegetation as dominant saltmarsh vegetation community. In this study, four drag coefficient formulations were reapplied: "Garzon Q_{KC}", "Garzon Q_{Re}", "Anderson & Smith", and "Jadhav" formulations.

2.2.2. Model parameterisation using satellite-derived leaf area index (LAI)

In contrast to the default FSA-based model, the LAI-based model uses LAI as a single input value to characterise vegetation structure by representing the product of height, diameter, and density (FSA). To do this, we are considering several assumptions which allow remote-sensed LAI to be incorporated into the numerical model. Firstly, we assume shallow water conditions in which the wavelength (L) is much larger than the water depth ($L >> h$). Saltmarshes are generally located in areas that fulfil this requirement, in particular during storm conditions and for infra-gravity waves, as assumed here (van Liew *et al.*, 2012; Forbes *et al.*, 2015; Mury *et al.*, 2018).

Secondly, the model assumes that vegetation is emergent (which is a requirement for accurate estimation of LAI from satellite imagery). Satellite data collection during storm events when vegetation is submerged would not be possible and no longer applicable. Having emergent vegetation conditions, wave attenuation is mainly a function of water depth rather than actual vegetation height, as that defines the surface area of plants that interact with the waves. Here, the near-emergent condition is based on Nepf (2004) definition using the ratio (h/h_v) ranged between 1 and 1.43 in this study which act physically similar to fully emergent canopies (Garzon *et al.*, 2019a). With these assumptions, the rate of wave energy attenuation due to vegetation can be rewritten:

$$\varepsilon_v = \frac{3}{2\sqrt{\pi}} \rho C_d \boldsymbol{\gamma}_v k \left(\frac{kg}{2\sigma} \right)^3 {H_{rms}}^3 \quad (2)$$

where we defined a new parameter γ_v that depends on water depth (h) rather than vegetation height, stem diameter (b_v), and plant density (N_v) and assume it is represented by the leaf area index obtained from satellite imagery:

$$\gamma_v = h\, b_v N_v \approx LAI \quad (3)$$

However, the spatial variation in LAI can only be attributed to either stem diameter or density as model input. Here, we opt to incorporate the LAI as vegetation diameter, while we assigned the density to be unity. We also applied dummy values to the model input vegetation height (10 m) to ensure emergent vegetation conditions. The uncertainty associated with these assumptions was verified for a broad range of emergent vegetation heights and wave conditions. Direct model results of wave attenuation with identical model runs with directly specified vegetation properties (vegetation height, diameter and density inputs) were also tested for significant variations in the model results. Differences between model runs were found negligible (< 1%) and thus this simplification is considered acceptable.

Finally, the model uses a constant drag coefficient C_d as we focus on modelling wave attenuation during storm conditions (with relatively high *Re* and *KC*-numbers) under which C_d has previously been shown to become relatively insensitive of *Re* and/or *KC* (e.g. van Loon-Steensma *et al.*, 2014). LAI values do not provide information on plant diameter either which is usually required as input for empirical formulations (e.g. Mendez and Losada, 2004; Pinsky *et al.*, 2013; Garzon *et al.*, 2019a). However, as shown in Equation 3, LAI accounts for the frontal surface area (FSA) that is expressed in terms of stem height, diameter, and density and makes it suitable for substitution in the formula. Overall, under the previous assumptions, the LAI-based model is convenient since it allows maintenance of the vegetation model implementation in its current form for a wide utilisation based on specific vegetation structure characteristics.

3. Results

3.1. Model calibration (US site)

3.1.1. Background and vegetation data

FSA-based and LAI-based models were calibrated using vegetation and hydrodynamic data reported by Garzon *et al.* (2019b) in a saltmarsh located on the eastern shore of Virginia National Wildlife Refuge on the southern tip of the Delmarva Peninsula which is bordered by the Chesapeake Bay, US (Figure 1). In this study area, the mean tidal amplitude is 0.9 m and is influenced by a 100-m-wide channel, the barrier island structure, and high-energy waves from the open ocean (Garzon *et al.*, 2019b). Four wave sensors recorded total pressure at 4Hz made up of hydrostatic pressure, dynamic wave pressure and atmospheric pressure from September 24th to October 1st in 2015. Plus, one hundred and twenty-nine sea state conditions including significant wave height (H_s), wave peak period (T_p), and water depth (h), were simulated from the offshore to the backside of the saltmarsh. Detailed information of the field deployment, transect utilised and wave sensor locations can be found in Garzon *et al.* (2019a) in which authors concluded that saltmarshes should be included in coastal defences even under storm conditions.

Since the focus of this paper is modelling wave attenuation during storm conditions, only incoming conditions with significant wave heights (calculated from the variance of water surface elevation spectrum from the wave data) greater than 0.3 m were considered. Thus, we selected a subset of 15 wave conditions as independent events with significant wave height (H_s), T_p ranging 2.5-5.9 seconds, and h ranging 0.7-0.9 m at sensor 2 (Figure 1c) to determine the range of wave attenuation rates in terms of H_s decay along the transect and considering drag coefficient (C_d) as a calibration parameter for both FSA and LAI models. The cross-shore distance (x) is defined along with the profile (Figure 1d), where x = 0 m at the leading edge of the saltmarsh areas, and H_s decay due to vegetation drag is measured as a function of distance.

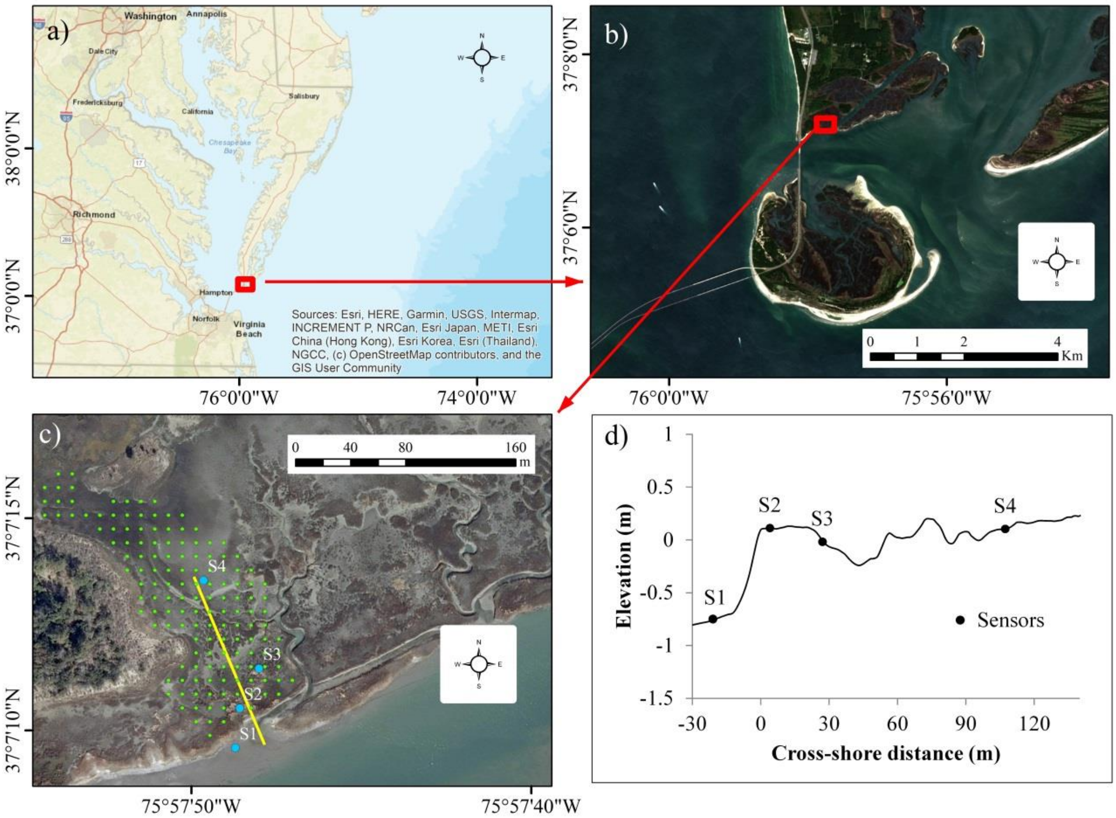

Figure 1 Chesapeake study site
(a) Location of Chesapeake Bay in the USA, background image corresponds to Esri, DigitalGlobe, GeoEye, Earthstar Geographics, CNES/Airbus DS, USDA, USGS, AeroGRID, IGN, and the GIS User Community. (b) Location of Chesapeake Bay study site: Eastern Shore, background image corresponds to Vertical Aerial Photography (Environment Agency, 2020c), corresponds to the red square in panel a. (c) Location of wave sensors (blue dots), normal transect used for the modelling (yellow line), and centre of 10 m pixels of LAI from satellite imagery (green dots), background image corresponds to OrthoImagery (USGS, 2020), corresponds to the red square in panel b. (d) Topo-bathymetric transect and location of the wave sensors.
Source: Based on data of Chesapeake site

To assign the vegetation structure component of the FSA-based model, we used FSA as the product of height (h_v), diameter (b_v), and density (N_v) based on 18 samples from the study of Paquier *et al.* (2016) which was also used by Garzon *et al.* (2019a). For the LAI-based model, we obtained LAI values at 165 nearby locations of 10 m by 10 m pixels from Sentinel-2 MSI (Figure 1c) on the closest available date to the storm event (14/09/15). Finally, basic descriptive statistics were calculated for all vegetation parameters (Table 1), and constant mean values across the vegetation field were used as input into the XBeach model. FSA seems to show more variability than LAI due to its limited sample (18 samples), that is why mean FSA is varying by a factor of 2 related to mean LAI (Table 1).

Table 1 Descriptive statistics of vegetation parameters.
Chesapeake Bay field site (Paquier *et al.*, 2016)

	h_v (m)	b_v (m)	N_v (m^{-2})	FSA	LAI
Min	0.53	0.004	270	0.572	0.417
Max	0.88	0.007	425	2.681	1.073
Mean	**0.71**	**0.005**	**344.7**	1.224	**0.636**
SD	0.22	0.0015	80	0.623	0.140
***Lower**	**0.58**	**0.0041**	**296.8**	0.704	**0.496**
***Higher**	**0.84**	**0.0059**	**392.6**	1.949	**0.776**

Bolded values were input into the XBeach model. SD: Standard Deviation. *For h_v, b_v, and N_v, lower and higher values were obtained as “Mean ± 0.6 x SD” while for LAI values as “Mean ± 1SD”.

The sensitivity of wave attenuation to variations in the drag coefficient and to the mean values of vegetation parameters shown in Table 1 is explored for both FSA-based and LAI-based models (see section 3.1.3). The range of C_d values obtained from the empirical formulations resulting from the FSA-based model was compared to constant C_d values from the LAI-based model. The FSA-based model used 4 relationships for C_d from the literature: 3 calibrated in the field and one in the laboratory, “Garzon Q_{KC}”, “Garzon Q_{Re}” formulations calibrated in the same marsh (Garzon *et al.*, 2019b). To consider the sensitivity to vegetation variability, we use the mean and the standard deviation (SD) values of vegetation input parameters (Lower and Higher in Table 1).

In the LAI-based model, the mean LAI value was used (Table 1) and the C_d was used as a calibration factor (the FSA-based model was not calibrated to our specific data) in which C_d value range from 0.9 to 2.9 with increments of 0.5. Then the optimal C_d value was obtained from selecting outcomes with the minimum error statistics including coefficient of determination (R^2), root mean square error (RMSE), scatter index (SCI), and relative bias (R. bias). The offshore water levels and waves were based on observations at station S1 (Figure 1c).

3.1.2. Comparing FSA-based and LAI-based models performance

In this section, we provide a calibration of the XBeach for the Chesapeake Bay site using 15 stationary wave conditions selected with significant wave heights (0.30 m – 0.38 m), wave peak periods (2.5 s – 5.9 s), and water depth (1.56 m – 1.81 m). The four selected C_d values from empirical formulations are used in the FSA-based model while constant C_d value is used in the LAI-based model. All previous parameters are also assumed constant across the transect.

Our results show that the significant wave height exponentially decreases as highlighted in Figure 2 for a representative case with the following offshore wave parameters: H_s = 0.31 m, T_p = 2.71, and mean water level of 0.89 m above MSL at sensor 2. Across all simulated cases, the simulated wave evolution using the calibrated LAI along the transect is similar to the FSA-based model in which the "Jadhav" formulation for C_d provides the best approximation. The other formulations that are considered all overpredict wave attenuation due to higher drag coefficient values, in particular the Garzon-KC formulation that leads to a roughly 50% lower wave height at sensor 4 (Figure 2) and also the largest error (Table 2).

Using the LAI-based model with a drag coefficient of C_d =1.9 (based on calibration with all 15 wave conditions), the wave height evolution is generally captured well by the model although it slightly overpredicts the attenuation rates for this particular condition (Figure 2).

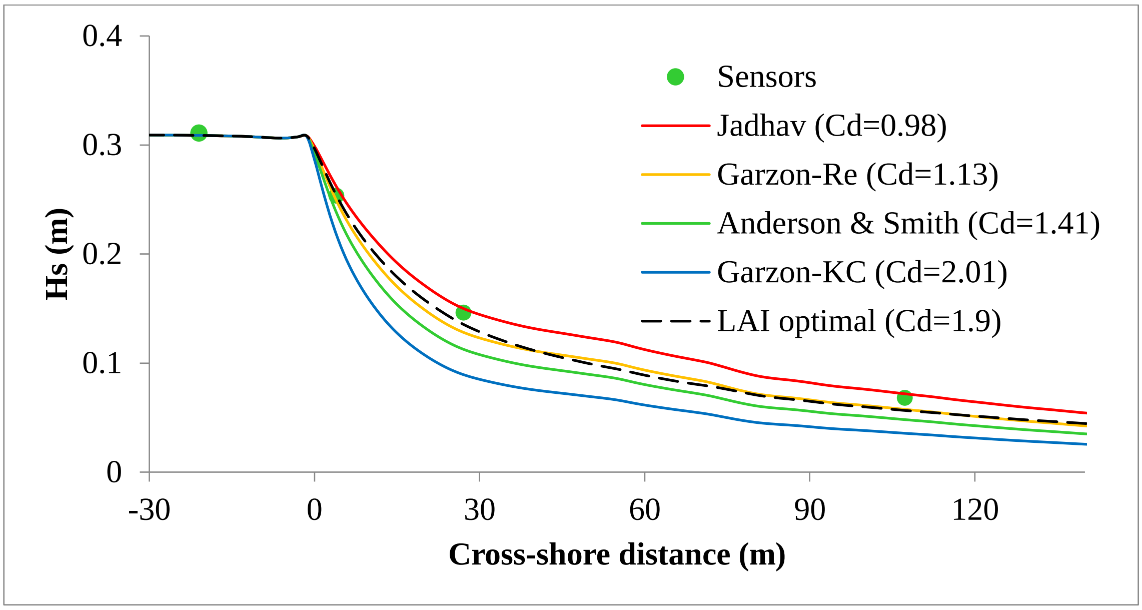

Figure 2 Wave attenuation along the saltmarsh in the Chesapeake Bay (US) Using a range of C_d empirical formulations in the FSA-based model (solid lines) and calibrated C_d in the LAI-based model (dashed line) for one representative wave condition (H_s = 0.31 m, T_p = 2.71). Sensors are shown as green dots.

The observed and modelled wave heights at sensor 2 to 4 for all 15 wave conditions are also compared for the LAI-based model with a calibrated drag coefficient (Figure 3). Predicted wave heights mainly overestimate the observations in sensor 2 while having a slight overestimation for small wave height and the underestimation for high wave heights in sensors 3 and 4, which may evidence that C_d should vary across the transect. This indicates that while a single calibrated value for C_d based on a range of wave conditions may lead to acceptable model results for some cases, it may either over- or underestimate wave attenuation rates for other cases. Here, the obvious alternative would be to calibrate the model for each individual wave condition to obtain case-dependent drag coefficients. This would, however, greatly limit the predictive capability of the model. Based on the 15 wave conditions, the calibrated drag coefficients range approximately from 1.3 – 2.5. Therefore, we could use constant C_d values across wave conditions in a predictive model.

To assess the performance of both FSA-based and LAI-based models, the error statistics are compared (Table 2). Overall, it is found that both models present similar accuracies in estimating wave attenuation by vegetation, in particular, when analysing sensors 3 and 4. The optimal C_d =1.9 of the LAI-based model and the Jadhav C_d (the most accurate) of the FSA-based models present similar RMSE, SCI, and relative bias values while having different R^2 values in sensors 3 and 4. However, the most accurate C_d (LAI-based) and Garzon-KC C_d (FSA-based) have similar RMSE, SCI, and Relative except for the R^2 value in sensor 2. Having similar incident wave values, constant C_d values are suitable with the bias errors found (slightly under predicting higher waves and over predicting lower waves).

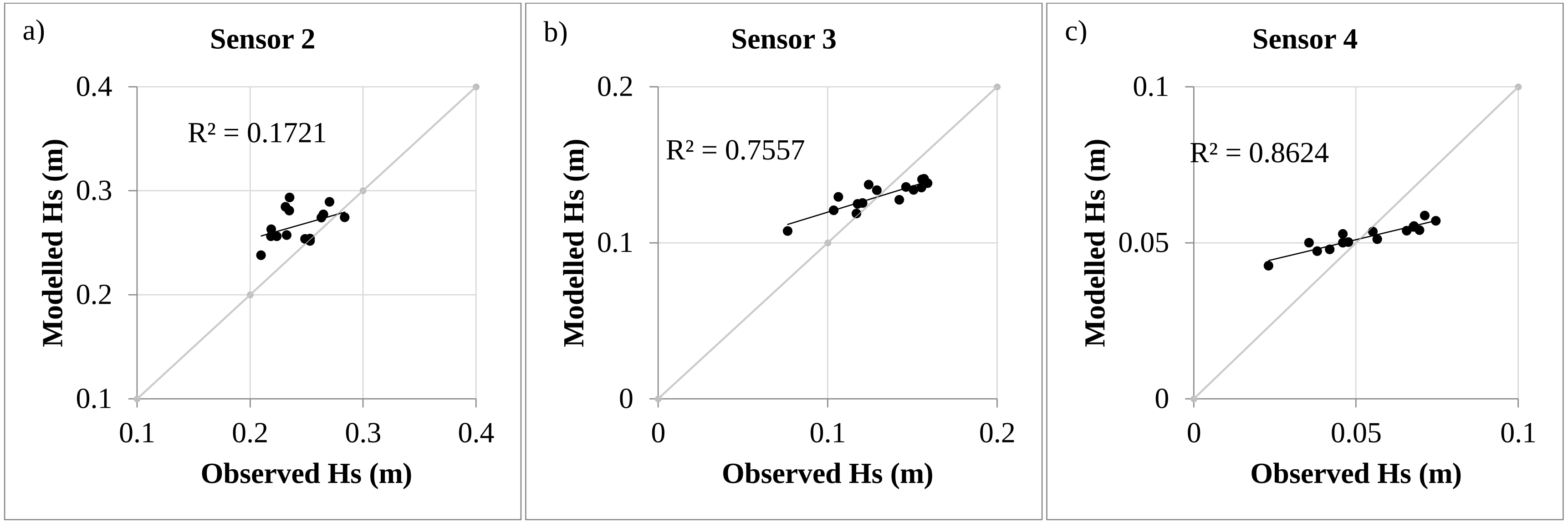

Figure 3 Comparison between observed and modelled significant wave height (H_s) at each sensor location
The subset of the 15 wave records under storm conditions using the LAI-based model

Table 2 Error statistics: empirical Cd (FSA-based) and constant Cd (LAI-based)

C_d	Sensor 2				Sensor 3				Sensor 4			
	R^2	**RMSE**	**SCI**	**R. bias**	**R^2**	**RMSE**	**SCI**	**R. bias**	**R^2**	**RMSE**	**SCI**	**R. bias**
Garzon-KC	**0.71**	0.04	0.16	0.15	0.84	0.06	0.47	0.46	0.86	0.03	0.55	0.51
Garzon-Re	0.56	**0.01**	**0.06**	**-0.01**	**0.85**	0.03	0.20	0.19	**0.87**	0.01	0.25	0.19
Smith	0.63	0.02	0.07	0.05	0.84	0.04	0.31	0.30	**0.87**	0.02	0.37	0.33
Jadhav	0.51	0.02	0.09	-0.07	0.74	**0.01**	**0.11**	**0.07**	0.68	**0.01**	**0.16**	**0.04**
C_d =1.9 (LAI)*	0.17	0.03	0.13	-0.10	0.76	0.02	0.12	0.01	0.86	0.01	0.21	0.04

The coefficient of determination (R^2), the root mean square error (RMSE), the scatter index (SCI), and the relative bias (R. bias) are shown.
*Drag coefficient in the LAI-based model.

3.1.3. Sensitivities of wave attenuation to C_d and vegetation properties

Overall, both the FSA-based and the LAI-based models have similar sensitivity to variations of drag coefficient (C_d), as well as, variations of height, diameter, density, and LAI. The C_d values calculated by XBeach in the FSA-based model vary from 1 to 2 which resulted in a range of wave evolution predictions (Figure 2). A similar range of C_d -values is used in the LAI-based model to assess the model sensitivity, showing that using a drag coefficient equal to the calibrated value minus or plus one results in about 50% lower or higher wave heights at sensor 4, respectively (Figure 4).

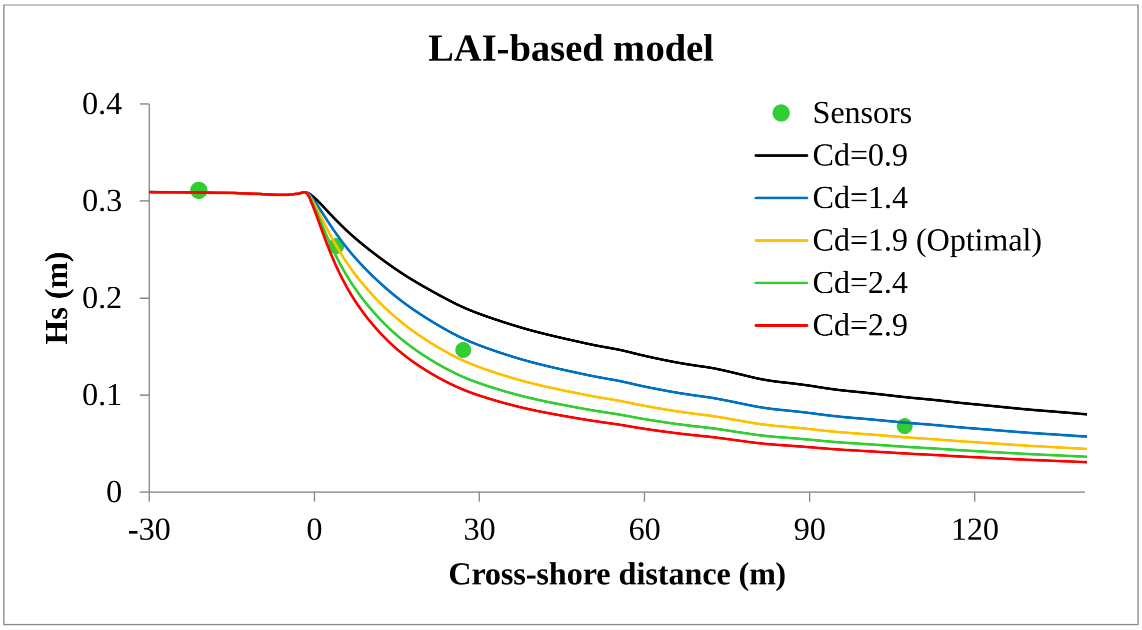

Figure 4 Wave attenuation using constant C_d values in the LAI-based model
Using a range of C_d constant values (solid lines) for one representative wave condition (H_s = 0.31 m, T_p = 2.71). Sensors are shown as green dots.

The range of estimated wave height across the saltmarsh for a range of vegetation properties is determined (grey areas in Figure 5) using both models. Based on the mean and standard deviation (SD) values in Table 1, the FSA-based model uses the mean and the mean ± 0.6 x SD of height, diameter, and density as inputs while the LAI-based model uses the mean and the mean ± 1SD of LAI as input. All previous input parameters are assumed constant across the saltmarsh.

The FSA-based model produces a wider range of estimated wave heights than the LAI-based model (Figure 5). In other words, the combined uncertainties of height, diameter, and density of the FSA-based model produce substantially higher uncertainty in wave attenuation predictions compared to the effect of the single uncertainty of LAI of the LAI-based model. Overall, the LAI-based model produces less uncertainty than the FSA-based model related to C_d and vegetation variability. The C_d used in the FSA-based model (Jadhav's = 0.98) is around half of the C_d used in the LAI-based model

(1.9). However, when running simulations with the same C_d in both models, the uncertainties found remain very similar as shown in Figure 5.

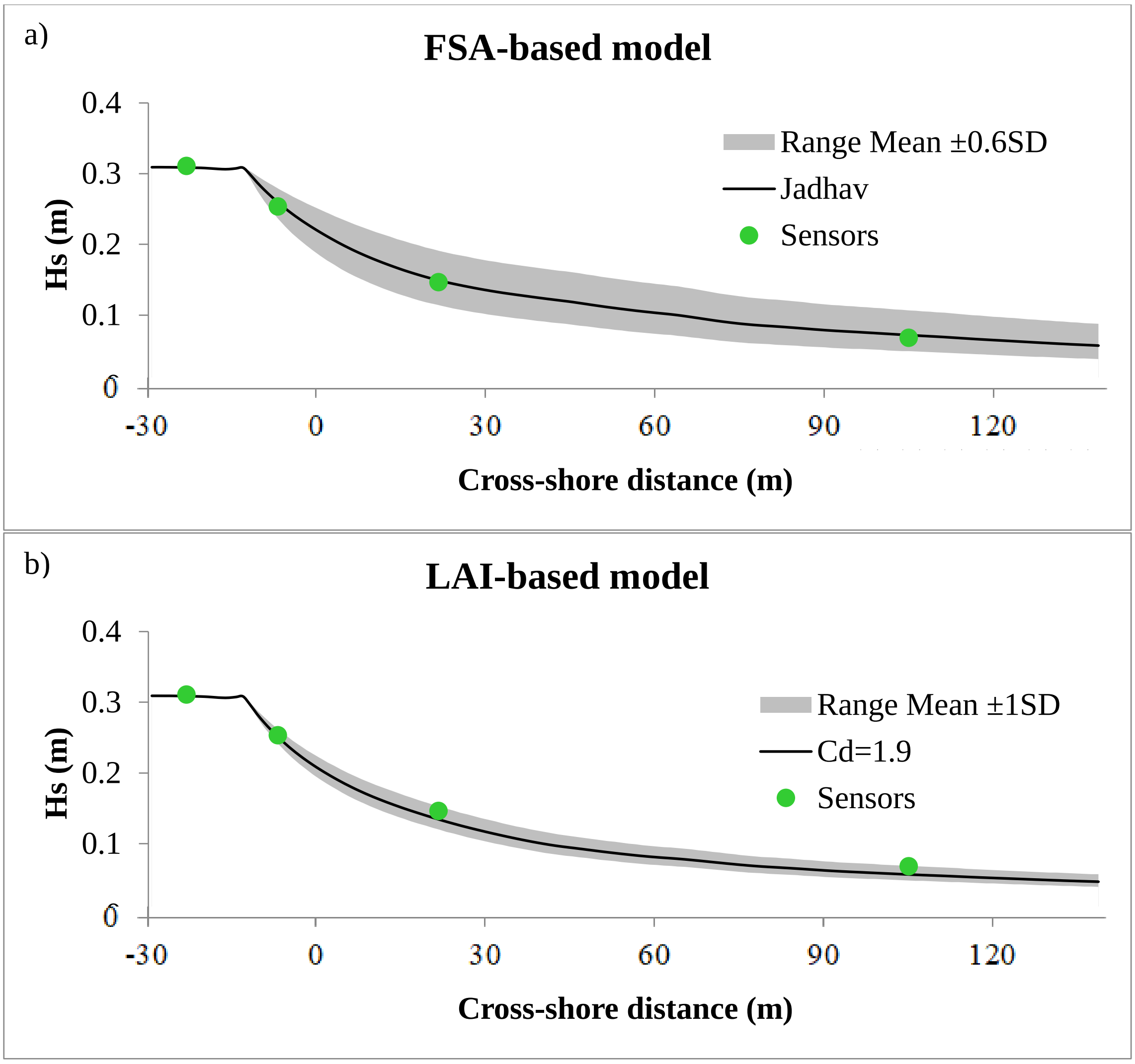

Figure 5 Wave attenuation sensitivity due to vegetation parameters
Using one lower and one higher value of (a) height, diameter, and density (FSA-based model) and (b) LAI (LAI-based model) on one representative wave condition (H_s = 0.31 m, T_p = 2.71). Sensors are shown as green dots.

3.2. Model application (UK site)

3.2.1. Site description and 2D model settings

Further applicability of the LAI-based model to other saltmarsh communities and geographical locations is relevant for generalisation purposes. This study selected a UK saltmarsh site to model a hypothetical future condition with a specific storm event as an example of model application. To explore the capacity of two types of saltmarshes, natural and artificial (in particular, a nature-based scheme referred to as "managed realignment"), to attenuate wave energy with and without vegetation, during summer and winter seasons and thus provide coastal flood protection, a two-dimensional model was used in the UK site. This study is not intended to provide more accurate results than using field-based methods to determine FSA, instead, the key goal is to have a fast and cheap methodology using remote sensing.

The study site is located in Brancaster on the North Norfolk coastal strip (Figure 6), on the western coast of England, and consists of a freshwater grazing marsh (Myatt-Bell *et al.*, 2002). Both natural and artificial saltmarshes are located in the same marsh platform (approximately same elevation) with similar morphological characteristics and subject to identical hydrodynamic conditions. Hence it can be considered that any differences in wave attenuation in both sites are caused by differences in saltmarsh vegetation properties. Currently, these saltmarshes are sheltered from storm waves by 4-5 meters high artificially armoured sand dunes (Myatt-Bell *et al.*, 2002) (Figure 6d). However, government authorities are planning to remove the dunes in future in order to restore the natural habitat and provide protection through the saltmarsh. Here, we tested the scenario without these dunes in which saltmarshes will be directly impacted by waves.

To evaluate the impact of saltmarsh vegetation on wave attenuation between artificial and natural saltmarshes and between seasons, a storm surge event with high water level of 2.56 m at Ordnance Datum - OD, significant wave height of 2.80 m, and peak period of 14.0 s, recorded in November 2008 (Environment Agency, 2014) in the Brancaster study site was simulated that would reach saltmarsh vegetation in the case of no dunes. Wave data were extracted from the Acoustic Wave and Current meter (AWAC) located offshore of Scolt Head Island (S9N; Figure 6c).

The offshore boundary of the grid domain lies approximately on the AWAC location at 20 meters water depth. The lateral boundaries were set up as Neumann boundaries. For all other XBeach settings, default values were used. The grid had dimensions of 7 x 5 km and a cross-shore and long-shore resolution of 10 m. The model bathymetry was extracted from Digimap Service (Digimap, 2020) operated by EDINA at the University of Edinburg formed by seabed elevation relative to the Chart datum (CD) that was changed into Ordnance Datum (OD) for our case study. Topography data were extracted from the SurfZone Digital Elevation Model (DEM) generated by the Environment Agency (UK) in 2014.

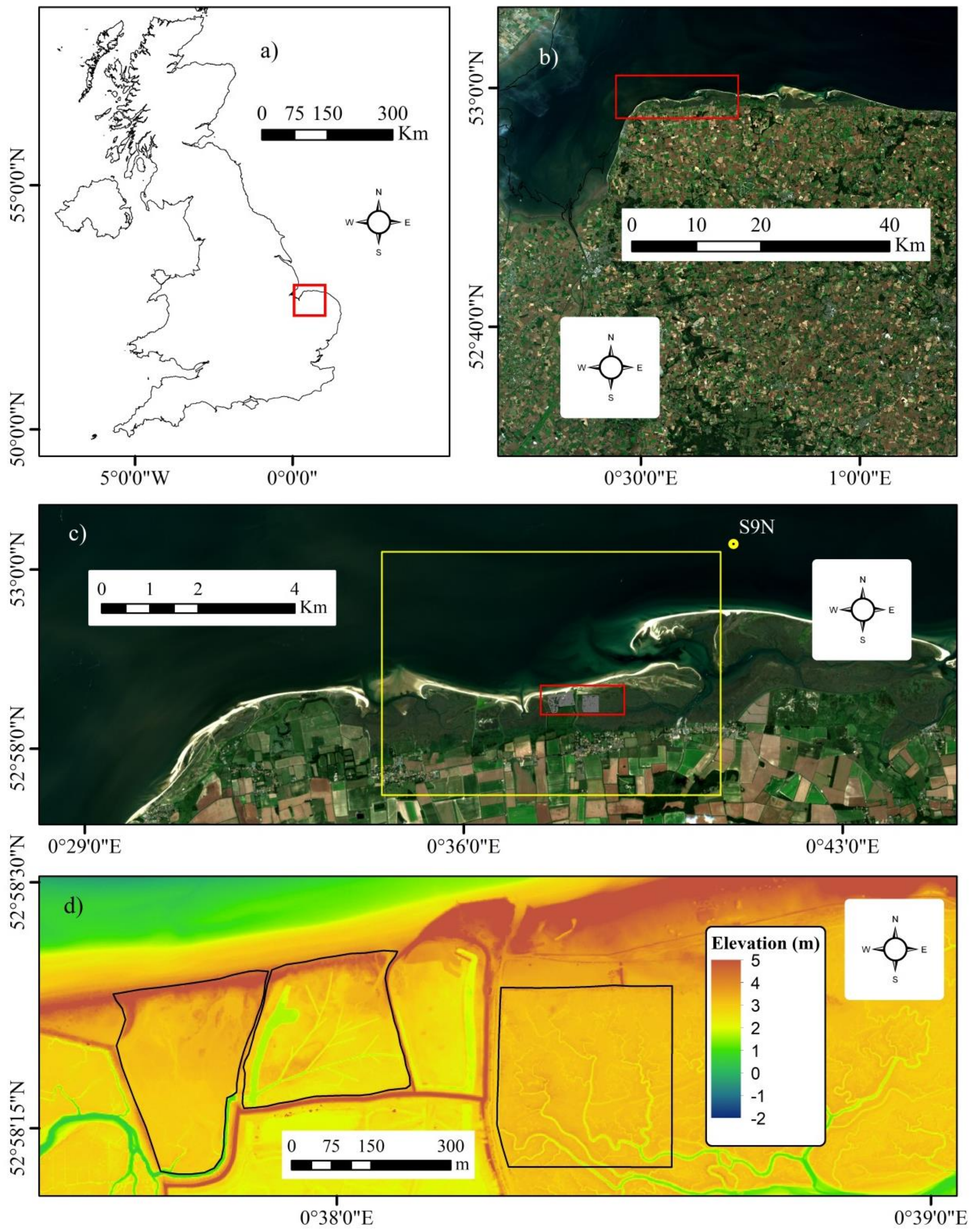

Figure 6 Brancaster study site

(a) United Kingdom (b) North West Norfolk coast, corresponds to the red square in panel a. (c) Brancaster Bay, corresponds to the red square in panel b, location of AWAC S9N instrument (53º 00.027’N; 00º 41.065’ E; 5m depth CD) and the XBeach model domain (7 x 5 km yellow rectangle, at 10 m grid resolution). (d) Location of Brancaster West Marsh (middle polygon), two natural saltmarsh areas (side polygons), corresponds to the red square in panel c, elevation at Ordnance Datum Newlyn (OD): the sea level height datum in the UK. The middle marsh and the marsh on its left were used to

calculate wave attenuation by vegetation. Background image corresponds to RGB Sentinel-2 imagery from ESA (2021) in panels b and c.
Source: Based on data from Environment Agency (2020)

LAI values were derived from Sentinel-2 MSI imagery from July 23rd, 2019 for summer and January 29th, 2020 for winter seasons based on an empirical Gaussian processes regression (GPR) model calibrated for that site (R^2= 0.99 and 0.89 respectively) from Figueroa-Alfaro *et al.* (2021). Finally, LAI values were classified into 6 classes (A-F) (Figure 7) based on the “natural breaks” classification and then the mean of each class (Table 3) was input in the model.

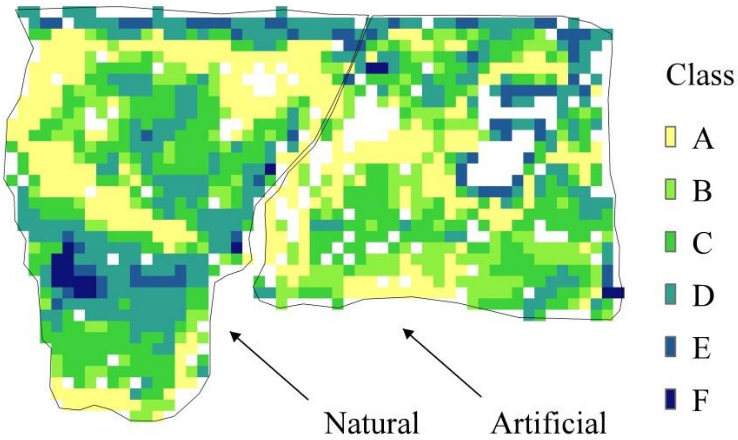

Figure 7 Remote sensed LAI classes of natural and artificial saltmarshes
LAI is classified from low (A) to high (F) values are their distribution within the saltmarshes are shown. White spaces contain no vegetation.

Table 3 Mean remote-sensed LAI values used as input in the model

Class		A	B	C	D	E	F
Surface (%)		26%	17%	28%	23%	5%	1%
LAI (m^2/m^2)	Summer	0.51	0.86	1.25	1.66	2.08	2.54
	Winter	0.49	0.71	0.86	1.03	1.23	1.43

Surface (%) shows the coverage per each saltmarsh class (A - F)

3.2.2. Potential outcomes of wave attenuation estimations

The LAI-based model, when calibrated, provides good results for the Chesapeake site based on data and comparison to the FSA-based model (Figure 2). Given the suitability of our LAI-based model, we can transfer this to another location with the type of vegetation and wave conditions for this site, using the calibrated C_d to assess the efficacy of managed realignments such as our Brancaster site (artificial saltmarsh) which was created to provide flood protection as a nature-based mitigation strategy. The storm simulated is a potential event during winter months and the following hydrodynamic data (historically recorded) are used; water level elevation (2.56 m at Ordnance Datum - OD) as the high water level, significant wave height (2.80 m), peak period (14.0 s), and wave direction (360º) which is approximately normally-incident. To have a better visualisation of the wave attenuation effect due to vegetation, the cross-shore direction is showed as x-axis (Figures 8 and 9) by flipping 90 degrees anti-clockwise relative to Figure 7. Seasonality will also influence flood protection provided since vegetation structure, expressed as LAI, varies from season to season. Saltmarsh vegetation is fully grown in summer and some senescent in winter.

XBeach is run for a future scenario in which the artificially armoured sand dunes fronting the saltmarsh vegetation are removed (Myatt-Bell *et al.*, 2002) allowing saltmarshes to attenuate wave energy rather than the dunes. Three scenarios are simulated: without vegetation, with summer vegetation and with winter vegetation. The root-mean-square wave height (H_{rms}) for sea-swell waves (H_{rms_ss}) is based on the wave energy output; the infra-gravity (IG) wave height (H_{rms_ig}) is derived from the water level variance, and wave setup is calculated as the difference between the simulated mean water level across the domain and the offshore mean water level. Finally, the absolute and relative wave height and wave setup differences between non-vegetated scenario and vegetated scenario (both summer and winter vegetation) are assessed.

Under the non-vegetated scenario, once the incident wave height is mainly reduced to 0.13 m due to topography, the sea-swell height at the saltmarsh offshore boundary is reduced substantially from approximately 0.13 to 0.05 m due to depth-induced wave breaking (Figure 8a). Under vegetated scenarios, there is an additional reduction in sea-swell wave height of up to 0.08 m, which is similar in summer (Figure 8b) and winter (Figure 8c). Most of the energy reduction occurs near the leading edge of the marsh due to depth-limited wave breaking. The additional wave height reduction due to saltmarsh vegetation equals around a maximum of 75% of the wave height on the inland portion of the saltmarsh (Figure 9a and 9b). When comparing natural and artificial saltmarshes, both show similar wave height reduction. Interestingly, there are slightly higher waves immediately on the offshore boundary of the saltmarsh vegetation that might be related to an increment of the local water depth associated with IG wave reflection (Figure 8d) as well as an increase of wave setup (Figure 8g), thereby reducing depth-induced wave breaking of sea-swell waves.

Infra-gravity (IG) waves can become important contributors to the total nearshore water level during storm conditions (van Thiel de Vries *et al.*, 2008). Under the non-vegetated scenario, there are two areas with IG wave heights up to 0.7 m in the artificial marsh while IG wave height reduction is a maximum of 0.3 m in the natural saltmarsh area (Figure 8d). The IG wave height is substantially reduced by saltmarsh vegetation during both seasons with a wave height reduction up to 0.21 m in the artificial saltmarsh while about 0.07 m reduction is found within the natural saltmarsh (Figure 8e and 8f). A small increase in IG wave height is also found at the offshore boundary of the saltmarshes which is due to IG wave reflection off the saltmarsh leading edge (Figure 8e and 8f). Notably, around 30% of IG wave height is reduced due to saltmarsh vegetation on both seasons (Figure 9c and 9d). Behind the saltmarshes, there is also a deeper area (non-vegetated in the model) in which IG waves are being reflected back and forth (resonance).

The wave setup (increase in nearshore mean water level due to wave breaking) reaches up to 0.49 m at the offshore boundary of both saltmarshes and decreasing more rapidly in the artificial saltmarsh than in the natural saltmarsh areas, under the non-vegetated scenario (Figure 8g). Similar to IG waves, wave setup is substantially decreased by saltmarsh vegetation with a reduction up to 0.12 m in the artificial saltmarsh while approximately 0.03 m reduction is shown in the natural saltmarsh. Setup is much smaller in the natural saltmarsh without vegetation and this reduction may be related to the bathymetry-topography. There is also a small increase in wave setup at the offshore boundary of the saltmarshes followed by a small decrease (Figure 8h and 8i). Similar to the attenuation of IG waves, around 30% of wave setup is reduced but only in the artificial saltmarsh while the natural marsh provides relatively small attenuation (Figure 9e and 9f). The attenuation of wave setup within the saltmarsh leads to lower mean water levels directly onshore (approximately 0.05 m).

Overall, our results show that the artificial saltmarsh provides similar rates of wave attenuation as a natural saltmarsh in terms of sea-swell wave height during both seasons, meaning the vegetation scheme can effectively provide wave height reduction. Saltmarshes are also able to attenuate IG wave energy and wave setup, providing additional risk reduction. In comparison, the artificial saltmarsh (having greater IG energy to start with) tends to produce slightly more attenuation than the natural saltmarsh in terms of IG wave height and wave setup during both seasons (Figure 8 and 9). Given that validation data is not available, our result are expressed as relative wave dissipation due to vegetation.

557

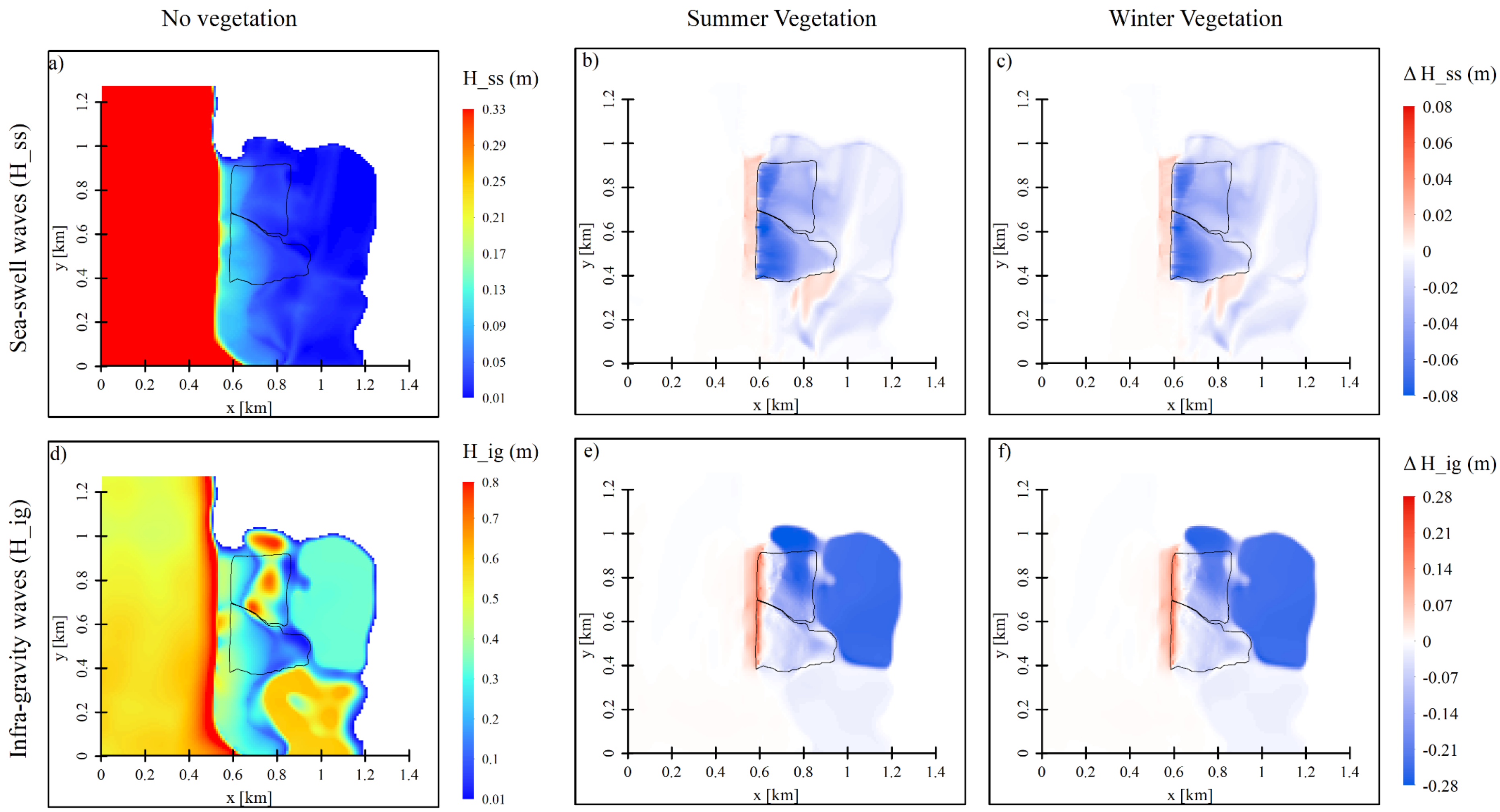

No vegetation
Summer Vegetation
Winter Vegetation
Sea-swell waves (H_ss)
Infra-gravity waves (H_ig)
a)
b)
c)
d)
e)
f)
H_ss (m)
0.33
0.29
0.25
0.21
0.17
0.13
0.09
0.05
0.01
Δ H_ss (m)
0.08
0.06
0.04
0.02
0
-0.02
-0.04
-0.06
-0.08
H_ig (m)
0.8
0.7
0.6
0.5
0.4
0.3
0.2
0.1
0.01
Δ H_ig (m)
0.28
0.21
0.14
0.07
0
-0.07
-0.14
-0.21
-0.28
x [km]
y [km]

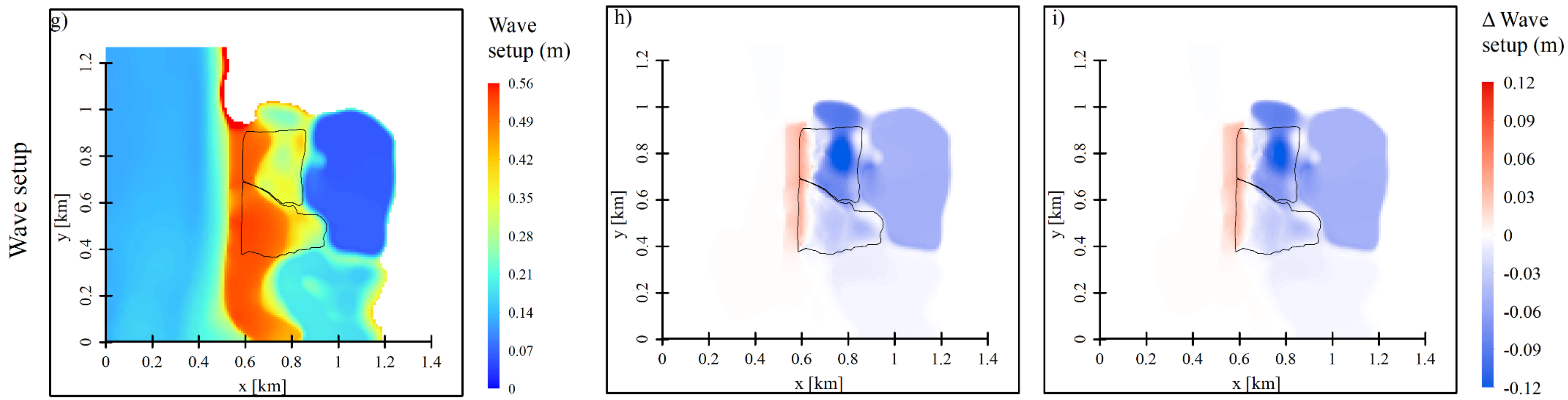

Figure 8 Wave attenuation at Brancaster site

Wave height decay of sea-swell waves (a) and infra-gravity waves (d) and variation of wave setup (g). Differences between simulations with summer vegetation and without vegetation (b, e, and h) and between simulations with winter vegetation and without vegetation (c, f, and i) of sea-swell waves (a, b, and c), infra-gravity waves (d, e, and f), and wave setup (g, h, and i).

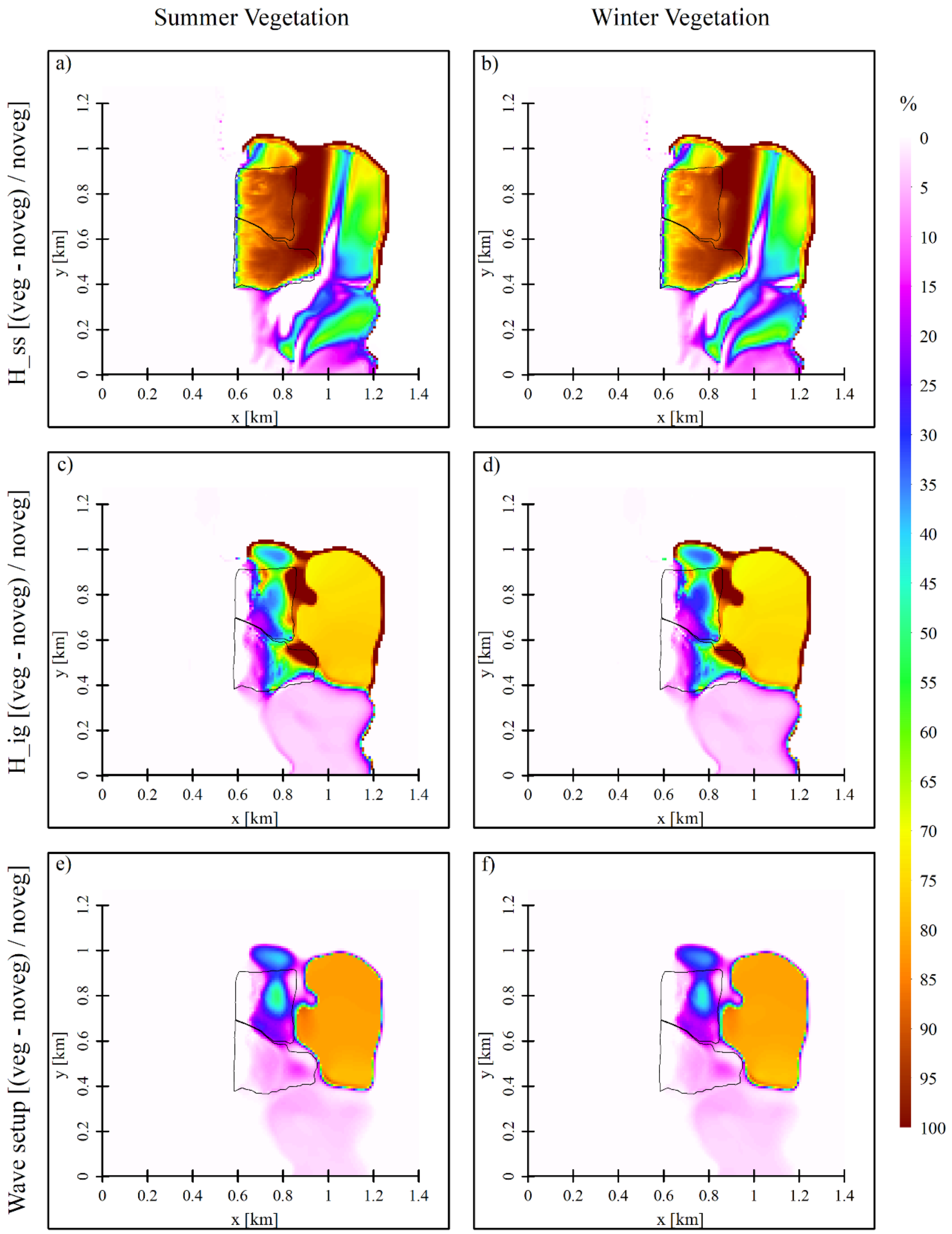

Figure 9 Relative wave attenuation at Brancaster site

Relative wave height differences of sea-swell waves (a, b), and infra-gravity waves (c, d), and the relative difference in wave setup (e, f) between simulations with vegetation in summer (a, c, and e) and winter (b, d, and f) compared to the scenario without vegetation.

4. Discussion

4.1. Comparison of FSA-based and LAI-based models

Most studies of wave attenuation by vegetation focus on the determination of the drag coefficient of vegetation (C_d) (Jadhav *et al.*, 2013) that must be calibrated in advance to be used in hydrological models (Mendez and Losada, 2004). Currently, empirical formulas are incorporated from literature to obtain C_d (Marsooli *et al.*, 2017) based on local plant properties, and hydrodynamic and topographical characteristics (Yang *et al.*, 2012). Our results using FSA as the vegetation input show that the range of wave attenuation derived from the four empirical formulations of C_d (for the same vegetation species) in the Chesapeake Bay study site spans the field-observed wave attenuation values (Figure 2) and the Jadhav formulation most accurately simulates wave heights for the Chesapeake Bay dataset of Garzon *et al.* (2019a). It has been demonstrated by Garzon *et al.* (2019b) and again in this paper that the use of empirical formulations tends to be adequate to estimate wave attenuation; however, it requires wave and vegetation measurements to derive C_d as part of the estimations.

Our results using LAI as the vegetation descriptor assess a range of constant values of C_d in the calibration and identify an optimal C_d =1.9 (Figure 4). Overall, the error statistics on both FSA-based and LAI-based models seem to be very similar, meaning that the LAI-based model is an effective alternative to the FSA-based model. This gives an advantage to the LAI-based model because it uses one remote-sensed input parameter instead of three field-based inputs. In this way, it is possible to cover larger saltmarsh vegetation areas in which field data might be difficult to obtain. Likewise, time consumed in field vegetation surveys can be minimized without losing significant model accuracy and provides more complete spatial coverage.

Nevertheless, some shortcomings of the LAI-based model should be considered in its application. As described in section 2.2.2, it is assumed hydrodynamic conditions are shallow water in low-lying coastal environments and near-emergent or emergent vegetation conditions where wave attenuation mainly relies on water depth. Emergent condition is also an assumption that may not always be valid, for instance, during a storm surge when entire marshes are submerged. As a result, the date of the data collection should be selected carefully by considering these conditions in shallow waters. Related to the assumption of C_d, the physical meaning of this coefficient is already complex when using the field-based approach (as we are assuming plants to be rigid cylinders) and become more complex with LAI representing FSA. Given that our paper also assumed a constant C_d value, further investigations are needed to estimate this value and apply the LAI-based model in many sites to validate the method and provide more robust and accurate results based on the monitoring and management requirement of the specific study area.

4.2. Impact of variation of C_d and vegetation

Since the drag coefficient (C_d) is an essential parameter in wave attenuation by vegetation, it is important to consider its impact in wave attenuation modelling. Our results show that varying C_d produces significant (and comparable) uncertainty in both the FSA-based model (Figure 2) and the LAI-based model (Figure 4). One reason for the uncertainty of the FSA-based model is the uncertainty associated with the field-based vegetation parameters while the uncertainty of the LAI-based model depends on the uncertainty of a single parameter (LAI).

The FSA-based model incorporated C_d values from empirical formulations ranging from ~1 to ~2 (Figure 2) while the LAI-based model used constant C_d values from 0.9 to 2.9 (Figure 4), both covering similar areas of wave attenuation. In order to have similar wave attenuation conditions, the C_d values in the LAI-based model were selected from the optimal C_d value tested when matching the observed wave attenuation values in the field (Figure 2). That is why C_d = 1.9 and increments of 0.5 were chosen in the LAI-based model. Although there was not validation data for the UK site, this paper focused on the relative wave attenuation between non-vegetated and vegetated scenarios. Further studies may estimate C_d in the UK site for validated results as well as validating the method in many sites.

Some uncertainties in wave attenuation estimation are also due to the initial assumption of uniform vegetation properties (Foster-Martinez *et al.*, 2018). The traditional and most used model (FSA-based model) considers the height, diameter, and density of vegetation (Anderson and Smith, 2015; Marsooli *et al.*, 2016; Marsooli *et al.*, 2017). However, incorporating sampling variation (Table 1) leads to significant uncertainty in attenuation modelling based on FSA in the Chesapeake Bay study site. Wave attenuation prediction using the FSA-based model, therefore, has a higher uncertainty level than using a single LAI value measured from satellite imagery in the LAI-based model as our results evidence. Thus, LAI is measurement across the entire saltmarsh that can be more easily obtained compared to the FSA parameters. Overall, both methods require validation of C_d for different vegetation, locations, seasons, etc.

4.3. Wave attenuation modelling application in 2D

One of the main techniques to monitor managed realignments is ecological monitoring (Adnitt *et al.*, 2007) such as vegetation surveys to evaluate the establishment of saltmarsh vegetation. Managed realignments often take around 4-5 years or more to establish their vegetation. For example, restored saltmarshes in the Great Bay Estuary, US show plant colonisation may be achieved within 7 years (Morgan and Short, 2002). At the Brancaster study site, the scheme was created in 2002 (Rees and Burns, 2014); and so, it is hypothesised that its saltmarsh vegetation is fully established and contributes to wave attenuation as well as a natural saltmarsh. This is confirmed by our maps of the relative wave height variation of sea-swell waves (Figure 9a and 9b). Maps of wave attenuation of infra-gravity (IG) waves (Figure 9c and 9d) and wave setup (Figure 9e and 9f) mainly show higher wave attenuation on the restored saltmarsh (given the higher IG energy at the beginning) rather than in the natural saltmarsh, proving significant evidence of potential flood protection.

The level of wave attenuation of sea-swell waves due to saltmarsh vegetation seems to be higher at the offshore boundary of the vegetated field and partially due to depth limited breaking. Previous studies have shown an exponential decrease of wave height due to wave propagation when crossing a vegetation field (Yang *et al.*, 2012; van Wesenbeeck *et al.*, 2017) with idealised bottom topography (Parvathy and Bhaskaran, 2017). Similarly, our results show exponential wave attenuation starting at the offshore boundary of the saltmarshes. This pattern is also seen in 1D wave attenuation modelling in XBeach which displays the exponential wave height decay inside two marshes (Garzon *et al.*, 2019b) including the Chesapeake, US site.

Our results of sea-swell wave attenuation are important and confirm previous studies of wave attenuation (van Rooijen *et al.*, 2016; Ozeren *et al*., 2017) given that both IG waves and wave setup are affected by saltmarsh vegetation as well. Both contribute directly to the total near-shore water level but also have an indirect impact allowing more sea-swell wave energy to propagate through. Wave setup is also affected by vegetation on distinct coastal configurations (van Rooijen *et al.*, 2016). The slight increase in wave height on the offshore area seems to mainly occur due to IG waves. These waves appear to be partially reflected by the saltmarsh vegetation and create higher local water depths in which the sea-swell waves are able to travel to a small distance further because of the increased water depth.

Finally, some studies have found that seasonality also plays an important role since vegetation may be present or absent during winter in some environments (Reef *et al.*, 2018). The presence of vegetation in numerical models is essential in simulating hydrodynamic conditions in saltmarsh platforms (Ashall *et al.*, 2016) and, posteriorly, predicting wave attenuation on coastal environments over time. Garzon *et al.* (2019b) showed reduced protection against waves during winter than fall in saltmarshes in the Chesapeake Bay, US. However, another study found wave attenuation from *Spartina foliosa* (California cordgrass) did not significantly vary between summer and winter (Foster-Martinez *et al.*, 2018). Given that our study lacks validation data, our results found similar relative wave attenuation using summer and winter saltmarsh vegetation which are the same for both natural and artificial saltmarshes. The next step would be to validate our outcomes for this site. Further investigations may also explore other types of saltmarsh vegetation communities with different seasonal vegetation (annual or perennial plants) given that using LAI makes it easier to assess seasonality and relate it to wave attenuation.

4.4. General application for coastal risk assessments

Coastal managers may benefit from this method following several straight-forward steps. First, retrieval of remotely-sensed saltmarsh LAI from free and open-access Sentinel-2 MSI imagery. Although there are few studies of saltmarsh retrieval derived from Sentinel-2 (i.e. Darvishzadeh *et al.*, 2019), potential saltmarsh LAI may be retrieved from different saltmarsh communities. Usually, saltmarsh vegetation is made of mixed canopy but dominant species should be considered to be quantified in terms of LAI. Second, confirmation of the assumptions required for the LAI-based model. Saltmarshes are commonly found on low-lying coastal areas (Pontee and Parsons, 2009) having emergent vegetation and under shallow conditions (Shi *et al.*, 2016); as a result, these assumptions should be confirmed in most of the cases. Third, the direct application of the XBeach wave model. As described in our method (see section 2.2.2), the current code and settings of the XBeach model can be used to estimate wave attenuation using LAI as input representing vegetation structure of the saltmarsh.

In terms of drag coefficient (C_d), this parameter is relevant but complex to estimate since it depends on the hydrodynamic conditions and vegetation parameters such as stem height, diameter, and density (Shafer and Yozzo, 1998; Suzuki *et al.*, 2012; Marsooli *et al.*, 2016). In order to use our LAI-based method, it is ideal to use an already estimated C_d of the study site. However, if it is unknown, a constant value may be used such as the typical value of $C_d = 1$ (i.e. Van Loon-Steensma, 2014) for comparing relative alternatives. Finally, the output generated should be carefully interpreted. Although reduction of sea-swell waves can provide a good insight of wave attention, changes of infra-gravity waves and wave setup should be considered as complementary outputs. Likewise, the outputs need to be clarified under the assumptions described in the LAI-based model and they might not be valid under other conditions such as submerged vegetation, deep water (relative to the wave length), or large storm events where wave attenuation by vegetation is not significant.

5. Conclusions

Numerical models can be used to estimate and predict wave attenuation by vegetation. This is important for monitoring coastal environments that are particularly vulnerable to wave-induced flooding. Field-derived input data for the modelling such as structural parameters of vegetation are difficult to obtain, but remote sensing techniques offer a faster and cheaper way to obtain vegetation parameters such as LAI. We conclude that the use of LAI as a vegetation parameter in the proposed LAI-based wave attenuation model is a suitable alternative given its similar accuracy to the traditional FSA-based model which uses field data.

Uncertainties of vegetation input parameters in numerical modelling may influence uncertainties of the wave attenuation estimations. We identified that variation of C_d values has a slightly higher impact on wave attenuation in the FSA-based model rather than in the LAI-based model. Likewise, the former model is sensitive to plant properties of height, diameter, and density given the natural variability which is hard to measure and produced a moderate uncertainty on wave attenuation. In contrast, the LAI-based model partially generated low wave attenuation uncertainty due to the single remote-sensed LAI input, covering the spatial variability in the saltmarsh.

Our practical application using the LAI-based model evidences an easier and faster approach to obtaining structural parameters of saltmarsh vegetation that can be used as input in wave attenuation models such as XBeach. Predictions derived from modelling may support evidence to increase the implementation of natural-based flood control schemes such as managed realignments. In our study, there is evidence that the level of wave attenuation due to saltmarsh vegetation in the managed realignment is as effective as that seen in natural saltmarsh in terms of the wave height variation in wind-generated sea-swell waves. The Brancaster managed realignment also partially provides more wave attenuation than natural saltmarsh in terms of wave height of infra-gravity waves and wave setup because the artificial saltmarsh has more IG energy than the natural saltmarsh. This result may be site specific, as a result of the topography/bathymetry.

In this study, the seasonality does not have a prominent impact on wave attenuation estimations. The FSA-based model only gives measurements for a specific moment, similar to the LAI-based model. However, remotely-sensed LAI as a temporal input can easily provide estimates of seasonal variation of wave attenuation. Further investigation is required to explore the application of the LAI-based model to other types of saltmarsh communities and to other regions.

Acknowledgements

We are thankful to the European Space Agency for providing freely accessed Sentinel-2 MSI data. Juan Garzon would like to thank the Flood Hazards Research Lab (FHRL) at George Mason University that gently shared the field data collected in the Chesapeake Bay and acknowledge the financial support of the Portuguese Foundation of Science and Technology (FCT) through ALG-LISBOA-01-145-FEDER-028657 and UID/00350/2020 CIMA. This work was supported by the RCUK-President’s Doctoral

Scholar (PDS) Award (2017-20) in the Faculty of Humanities at the University of Manchester, United Kingdom.

Declaration of competing interest

The authors declare that they have no known competing financial interests or personal relationships that could have appeared to influence the work reported in this paper.

Appendices

Appendix A. Calibration of LAI-based model using H_s of the average of the 15 wave conditions

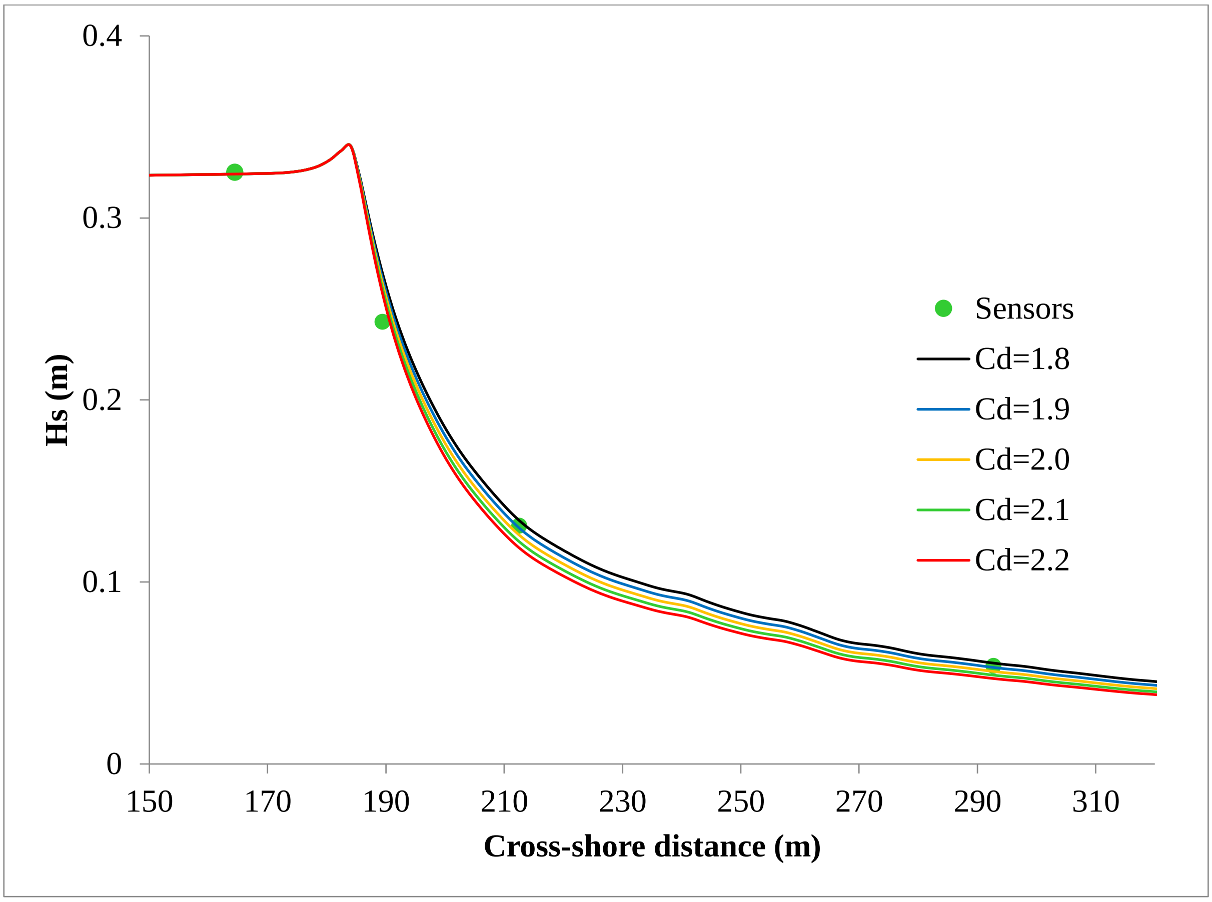

Figure A.1 Wave height decay using LAI-based model
Using a range of Cd constant values (solid lines) for one representative wave condition (Hs = 0.31 m, Tp = 2.71).

Table A.1 Error statistics using the LAI-based model
The coefficient of determination (R^2), the root mean square error (RMSE), the scatter index (SCI), and the relative bias (R. bias) are shown.

C_d	Sensor 2				Sensor 3				Sensor 4			
	R2	**RMSE**	**SCI**	**R. bias**	**R2**	**RMSE**	**SCI**	**R. bias**	**R2**	**RMSE**	**SCI**	**R. bias**
C_d =1.8	0.16	0.03	0.14	-0.11	0.75	0.02	0.13	-0.02	0.86	0.01	0.21	-0.01
C_d =1.9	0.17	0.03	0.13	-0.10	0.76	**0.02**	**0.12**	**0.01**	0.86	**0.01**	**0.21**	**0.04**
C_d =2.0	0.18	0.03	0.12	-0.09	0.76	0.02	0.13	0.04	0.87	0.01	0.23	0.08
C_d =2.1	0.19	0.03	0.11	-0.08	0.77	0.02	0.14	0.06	0.87	0.01	0.24	0.11
C_d =2.2	**0.19**	**0.03**	**0.10**	**-0.06**	**0.78**	0.02	0.16	0.09	**0.87**	0.01	0.26	0.15

References

Aberle, J. and Järvelä, J. (2013) ‘Flow resistance of emergent rigid and flexible floodplain vegetation', *Journal of Hydraulic Research*, 51(1), pp. 33–45. doi: 10.1080/00221686.2012.754795.

Adnitt, C. *et al.* (2007) '*Saltmarsh management manual'*. Environment Agency. Available at: http://publications.environment-agency.gov.uk/PDF/SCHO0307BMKH-E-E.pdf.

Anderson, M. E. and Smith, J. M. (2015) 'Implementation of Wave Dissipation by Vegetation in STWAVE', *US Army Corps of Engineers*. February, 2015. doi: 10.2464/jilm.61.507.

Ashall, L.M., Mulligan, R.P., Van Proosdij, D., and Poirier, E. (2016) 'Application and validation of a three-dimensional hydrodynamic model of a macrotidal salt marsh', *Coastal Engineering*. Elsevier B.V., 114, pp. 35–46. doi: 10.1016/j.coastaleng.2016.04.005.

Bréda, N. J. J. (2003) 'Ground-based measurements of leaf area index: A review of methods, instruments and current controversies', *Journal of Experimental Botany*, 54(392), pp. 2403–2417. doi: 10.1093/jxb/erg263.

Bridges, T. S. *et al.* (2015) 'Use of Natural and Nature-Based Features (NNBF) for Coastal Resilience', *US Army Corps of Engineers - Engineer Research and Development Center*. January, 2015. pp. 1–447. Available at: https://usace.contentdm.oclc.org/digital/collection/p266001coll1/id/3442/

Casa, R., Upreti, D. and Pelosi, F. (2019) 'Measurement and estimation of leaf area index (LAI) using commercial instruments and smartphone-based systems', *IOP Conference Series: Earth and Environmental Science*, 275, p. 012006. doi: 10.1088/1755-1315/275/1/012006.

Chen, J. M. *et al.* (2002) 'Derivation and validation of Canada-wide coarse-resolution leaf area index maps using high-resolution satellite imagery and ground measurements', *Remote Sensing of Environment*, 80(1), pp. 165–184. doi: 10.1016/S0034-4257(01)00300-5.

Clevers, J. G. P. W., Kooistra, L. and van den Brande, M. M. M. (2017) 'Using Sentinel-2 data for retrieving LAI and leaf and canopy chlorophyll content of a potato crop', *Remote Sensing*, 9(5), pp. 1–15. doi: 10.3390/rs9050405.

Darvishzadeh, R. *et al.* (2019) 'Analysis of Sentinel-2 and RapidEye for Retrieval of Leaf Area Index in a Saltmarsh Using a Radiative Transfer Model', *Remote*

Sensing, 11(6), p. 671. doi: 10.3390/rs11060671.

Davi, H. *et al.* (2006) ‘Estimation of forest leaf area index from SPOT imagery using NDVI distribution over forest stands’, *International Journal of Remote Sensing*, 27(5), pp. 885–902. doi: 10.1080/01431160500227896.

Day, J. W. *et al.* (2008) ‘Consequences of climate change on the ecogeomorphology of coastal wetlands’, *Estuaries and Coasts*, 31(3), pp. 477–491. doi: 10.1007/s12237-008-9047-6.

Delegido, J., Verrelst, J., Alonso, L., and Moreno, J. (2011) ‘Evaluation of sentinel-2 red-edge bands for empirical estimation of green LAI and chlorophyll content’, *Sensors*, 11(7), pp. 7063–7081. doi: 10.3390/s110707063.

Delegido, J. *et al.* (2015) ‘Brown and green LAI mapping through spectral indices’, *International Journal of Applied Earth Observation and Geoinformation*. Elsevier B.V., 35(PB), pp. 350–358. doi: 10.1016/j.jag.2014.10.001.

Digimap (2020) *Digimap*. Available at: https://digimap.edina.ac.uk/ (Accessed: 30 June 2020).

Environment Agency (2014) ‘*Sea State Report Norfolk*'. Year 3 and summary for October 2006 – September 2009. Shoreline Monitoring Group, Environment Agency (RP039/N/2014). Available at: https://www.coastalmonitoring.org/reports

Environment Agency (2020) ‘*Saltmarsh Extent & Zonation*’. Environment Agency. Available at: https://data.gov.uk/dataset/0e9982d3-1fef-47de-9af0-4b1398330d88/saltmarsh-extent-zonation

ESA (2015) ‘*Sentinel-2 User Handbook*’, European Space Agency (ESA) Standard Document, pp. 1–64. Available at: https://sentinel.esa.int/web/sentinel/user-guides/sentinel-2-msi/document-library/-/asset_publisher/Wk0TKajiISaR/content/sentinel-2-user-handbook

ESA (2021) '*Sentinel*'. European Space Agency - ESA 2000 - 2021. Available at: https://sentinels.copernicus.eu (Accessed: 29 June 2019).

Forbes, H., Ball, K. and McLay, F. (2015) '*Natural Flood Management Handbook*'. Scottish Environment Protection Agency (SEPA). doi: 10.13140/RG.2.1.4956.1444.

Foster-Martinez, M.R., Lacy, J.R., Ferner, M.C., and Variano, E.A. (2018) ‘Wave attenuation across a tidal marsh in San Francisco Bay’, *Coastal Engineering*.

Elsevier Ltd, 136(February), pp. 26–40. doi: 10.1016/j.coastaleng.2018.02.001.
Garzon, J. L. *et al.* (2019a) 'Wave Attenuation by Spartina Saltmarshes in the Chesapeake Bay Under Storm Surge Conditions', *Journal of Geophysical Research: Oceans*, 124(7), pp. 5220–5243. doi: 10.1029/2018JC014865.
Garzon, J. L., Miesse, T. and Ferreira, C. M. (2019b) 'Field-based numerical model investigation of wave propagation across marshes in the Chesapeake Bay under storm conditions', *Coastal Engineering*. Elsevier, 146(May 2018), pp. 32–46. doi: 10.1016/j.coastaleng.2018.11.001.
Gedan, K. B. *et al.* (2011) 'The present and future role of coastal wetland vegetation in protecting shorelines: Answering recent challenges to the paradigm', *Climatic Change*, 106(1), pp. 7–29. doi: 10.1007/s10584-010-0003-7.
Glass, E. M. *et al.* (2018) 'Potential of marshes to attenuate storm surge water level in the Chesapeake Bay', *Limnology and Oceanography*, 63(2), pp. 951–967. doi: 10.1002/lno.10682.
Green, E. P. *et al.* (1997) 'Estimating leaf area index of mangroves from satellite data', *Aquatic Botany*, 58(1), pp. 11–19. doi: 10.1016/S0304-3770(97)00013-2.
Jadhav, R. S., Chen, Q. and Smith, J. M. (2013) 'Spectral distribution of wave energy dissipation by salt marsh vegetation', *Coastal Engineering*. Elsevier B.V., 77, pp. 99–107. doi: 10.1016/j.coastaleng.2013.02.013.
Jalonen, J., Järvelä, J. and Aberle, J. (2013) 'Leaf area index as vegetation density measure for hydraulic analyses', *Journal of Hydraulic Engineering*, 139(5), pp. 461–469. doi: 10.1061/(ASCE)HY.1943-7900.0000700.
Jasinski, M. F. and Crago, R. D. (1999) 'Estimation of vegetation aerodynamic roughness of natural regions using frontal area density determined from satellite imagery', *Agricultural and Forest Meteorology*, 94(1), pp. 65–77. doi: 10.1016/S0168-1923(98)00129-4.
Jensen, J. R. *et al.* (2002) 'Remote sensing of biomass, leaf-area-index, and chlorophyll a and b content in the ACE basin national estuarine research reserve using sub-meter digital camera imagery', *Geocarto International*, 17(3), pp. 27–36. doi: 10.1080/10106040208542241.
Jonckheere, I. *et al.* (2004) 'Review of methods for in situ leaf area index determination Part I. Theories, sensors and hemispherical photography', *Agricultural and Forest*

Meteorology, 121(1–2), pp. 19–35. doi: 10.1016/j.agrformet.2003.08.027.

Karambas, T., Koftis, T., & Prinos, P. (2015) 'Modeling of Nonlinear Wave Attenuation due to Vegetation', *Journal of Coastal Research*, 32(1), p. 142. doi: 10.2112/jcoastres-d-14-00044.1.

Koch, E. W. *et al.* (2009) 'Non-linearity in ecosystem services: Temporal and spatial variability in coastal protection', *Frontiers in Ecology and the Environment*, pp. 29–37. doi: 10.1890/080126.

Korhonen, L., Hadi, Packalen, P., and Rautiainen, M. (2017) 'Comparison of Sentinel-2 and Landsat 8 in the estimation of boreal forest canopy cover and leaf area index', *Remote Sensing of Environment*. Elsevier Inc., 195, pp. 259–274. doi: 10.1016/j.rse.2017.03.021.

Leonardi, N. *et al.* (2018) 'Dynamic interactions between coastal storms and salt marshes: A review', *Geomorphology*. Elsevier B.V., 301, pp. 92–107. doi: 10.1016/j.geomorph.2017.11.001.

van Liew, M. W., Feng, S. and Pathak, T. B. (2012) 'Climate change impacts on streamflow, water quality, and best management practices for the shell and logan creek watersheds in Nebraska, USA', *International Journal of Agricultural and Biological Engineering*, 5(1), pp. 13–34. doi: 10.3965/j.ijabe.20120501.003.

van Loon-Steensma, J.M., Slim, P.A., Decuyper, M., and Hu, Z. (2014) 'Salt-marsh erosion and restoration in relation to flood protection on the Wadden Sea barrier island Terschelling', *Journal of Coastal Conservation*, 18(4), pp. 415–430. doi: 10.1007/s11852-014-0326-z.

Ma, G., Kirby, J. T., Su, S. F., Figlus, J., & Shi, F. (2013) 'Numerical study of turbulence and wave damping induced by vegetation canopies', *Coastal Engineering*. Elsevier B.V., 80, pp. 68–78. doi: 10.1016/j.coastaleng.2013.05.007.

Marsooli, R., Orton, P.M., Georgas, N., and Blumberg, A.F. (2016) 'Three-dimensional hydrodynamic modeling of coastal flood mitigation by wetlands', *Coastal Engineering*. Elsevier B.V., 111, pp. 83–94. doi: 10.1016/j.coastaleng.2016.01.012.

Marsooli, R., Orton, P. M. and Mellor, G. (2017) 'Modeling wave attenuation by salt marshes in Jamaica Bay, New York, using a new rapid wave model', *Journal of Geophysical Research: Oceans*, 122(7), pp.5689-5707.

doi.org/10.1002/2016JC012546.

Maza, M. *et al.* (2015) 'Large-scale 3-D experiments of wave and current interaction with real vegetation. Part 2: Experimental analysis', *Coastal Engineering*. Elsevier B.V., 106, pp. 73–86. doi: 10.1016/j.coastaleng.2015.09.010.

Mendez, F. J. and Losada, I. J. (2004) 'An empirical model to estimate the propagation of random breaking and nonbreaking waves over vegetation fields', *Coastal Engineering*, 51(2), pp. 103–118. doi: 10.1016/j.coastaleng.2003.11.003.

Morgan, P. A. and Short, F. T. (2002) 'Using functional trajectories to track constructed salt marsh development in the Great Bay Estuary, Maine/New Hampshire, U.S.A', *Restoration Ecology*, 10(3), pp. 461–473. doi: 10.1046/j.1526-100X.2002.01037.x.

Mury, A., Collin, A. and Etienne, S. (2018) 'Wave Attenuation Service by Intertidal Coastal Ecogeosystems in the Bay of Mont-Saint-Michel, France: Review and Meta-Analysis'. *Sixth International Conference on Estuaries and Coasts (ICEC-2018)*, Caen, France. August, 2018. Available at: https://doi.org/10.1007/978-981-15-2081-5_32

Myatt-Bell, L.B., Scrimshaw, M.D., Lester, J.N., and Potts, J.S. (2002) 'Public perception of managed realignment: Brancaster West Marsh, North Norfolk, UK', *Marine Policy*, 26(1), pp. 45–57. doi: 10.1016/S0308-597X(01)00033-1.

Nepf, H. M. (2004) 'Vegetated Flow Dynamics'. The Ecogeomorphology of Tidal Marshes. *Coastal and Estuarine Studies*, 59, pp. 137–163. doi: 10.1029/CE059

Nicholls, R. J. *et al.* (2018) 'Stabilization of global temperature at 1.5°C and 2.0°C: Implications for coastal areas', *Philosophical Transactions of the Royal Society A: Mathematical, Physical and Engineering Sciences*, 376(2119). doi: 10.1098/rsta.2016.0448.

Orlando, F. *et al.* (2016) 'Estimating Leaf Area Index (LAI) in Vineyards Using the PocketLAI Smart-App', *Sensors (Basel, Switzerland)*, 16(12), pp. 1–12. doi: 10.3390/s16122004.

Ozeren, Y., Wren, D. G. and Wu, W. (2014) 'Experimental Investigation of Wave Attenuation through Model and Live Vegetation', *Journal of Waterway, Port, Coastal, and Ocean Engineering*, 140(5), p. 04014019. doi: 10.1061/(asce)ww.1943-5460.0000251.

Ozeren, Y., Wren, D. and Wu, W. (2017) ‘Wave Setup on Vegetated Beach: Laboratory Experiments’, *Coastal Engineering Proceedings*, (35), p. 4. doi: 10.9753/icce.v35.currents.4.

Paquier, A.E., Haddad, J., Lawler, S., and Ferreira, C.M. (2016) ‘Quantification of the Attenuation of Storm Surge Components by a Coastal Wetland of the US Mid Atlantic’, *Estuaries and Coasts*. Estuaries and Coasts, 40(4), pp. 930–946. doi: 10.1007/s12237-016-0190-1.

Parvathy, K. G. and Bhaskaran, P. K. (2017) ‘Wave attenuation in presence of mangroves: A sensitivity study for varying bottom slopes’, *The International Journal of Ocean and Climate Systems*, 8(3), pp. 126–134. doi: 10.1177/1759313117702919.

Phan, L.K., Vries, van T. de, S.M., J., and Stive, M.J.F. (2015) ‘Coastal Mangrove Squeeze in the Mekong Delta’, *Journal of Coastal Research*, 300(May), pp. 233–243. doi: 10.2112/jcoastres-d-14-00049.1.

Pinsky, M. L., Guannel, G. and Arkema, K. K. (2013) ‘Quantifying wave attenuation to inform coastal habitat conservation’, *Ecosphere*, 4(8). doi: 10.1890/ES13-00080.1.

Pontee, N. I. and Parsons, A. (2009) ‘A review of coastal risk management in the UK’, *Proceedings of the Institution of Civil Engineers* (*ICE)*, Maritime Engineering, 163, pp. 31-42. doi: 10.1680/maen.2010.163.

Reef, R. *et al.* (2018) ‘The effect of vegetation height and biomass on the sediment budget of a European saltmarsh’, *Estuarine, Coastal and Shelf Science*, 202, pp. 125–133. doi: 10.1016/j.ecss.2017.12.016.

Rees, A. S. and Burns, O. (2014) ‘*Case study 47 . North Norfolk Coast*’. Environment Agency and Natural England. pp. 1–11. Available at: https://www.therrc.co.uk/sites/default/files/projects/47_northnorfolk.pdf

Roelvink, D. *et al.* (2015) ‘*XBeach Technical Reference: Kingsday Release*’, Model description and reference guide to functionalities. XBeach Technical Reference, pp. 1–141. doi: 10.13140/RG.2.1.4025.6244.

van Rooijen, A. A. *et al.* (2015) ‘Modeling of wave attenuation by vegetation with XBeach’, *E-proceedings of the 36th International Association for Hydro-Environment Engineering and Research (IAHR)World Congress*. The Hague, the

Netherlands. July, 2015. Available at: http://resolver.tudelft.nl/uuid:98a66b95-8fed-421a-9bfe-4ae978375dbe

van Rooijen, R. T. *et al.* (2016) 'Modeling the effect of wave-vegetation interaction on wave setup', *Journal of Geophysical Research: Oceans*, pp. 4341–4359. doi: 10.1002/ 2015JC011392.

Schepers L., Maris, T., Meire, P., and Temmerman, S. (2018) 'The Scheldt Estuary: An Overview of the Morphodynamics of Intertidal Areas', *Landscapes and Landforms of Belgium and Luxembourg*, World Geomorphological Landscapes, pp.281-296. doi.org/10.1007/978-3-319-58239-9_17

Shafer, D. J. and Yozzo, D. J. (1998) '*National guidebook for application of hydrogeomorphic assessment to tidal fringe wetlands*', Wetlands Research Program. Technical Report WRP-DE-16. US Army Corps of Engineers Waterways Experiment Station, pp. 1–79. Available at: https://apps.dtic.mil/sti/pdfs/ADA360802.pdf

Sheng, Y. P., Alymov, V. and Paramygin, V. A. (2010) 'Simulation of storm surge, wave, currents, and inundation in the outer banks and Chesapeake bay during Hurricane Isabel in 2003: The importance of waves', *Journal of Geophysical Research: Oceans*, 115(4). doi: 10.1029/2009JC005402.

Shepard, C. C., Crain, C. M. and Beck, M. W. (2011) 'The protective role of coastal marshes: A systematic review and meta-analysis', *PLoS ONE*, 6(11). doi: 10.1371/journal.pone.0027374.

Shi, B. W. *et al.* (2016) 'Role of wind in erosion-accretion cycles on an estuarine mudflat', *Journal of Geophysical Research: Oceans*, 122(1), pp. 193–206. doi: 10.1002/2016JC011902.

Smith, J. M. and Anderson, M. E. (2014) 'Limits of wetland wave dissipation', *Coastal Engineering Proceedings*, 1(34), waves.18, pp. 1–10. Available at: https://doi.org/10.9753/icce.v34.waves.18

Stockdon, H.F., Holman, R.A., Howd, P.A., and Sallenger, A.H. (2006) 'Empirical parameterization of setup, swash, and runup', *Coastal Engineering*, 53(7), pp. 573–588. doi: 10.1016/j.coastaleng.2005.12.005.

Sutton-Grier, A. E., Wowk, K. and Bamford, H. (2015) 'Future of our coasts: The potential for natural and hybrid infrastructure to enhance the resilience of our coastal communities, economies and ecosystems’, *Environmental Science and Policy*. Elsevier Ltd, 51, pp. 137–148. doi: 10.1016/j.envsci.2015.04.006.

Suzuki, T. *et al.* (2012) ‘Wave dissipation by vegetation with layer schematization in SWAN’, *Coastal Engineering*. Elsevier B.V., 59(1), pp. 64–71. doi: 10.1016/j.coastaleng.2011.07.006.

Tempest, J. A., Möller, I. and Spencer, T. (2015) ‘A Review of Plant-Flow Interactions on Salt Marshes: The importance of vegetation structure and plant mechanical characteristics'. *Wiley Interdisciplinary Reviews(WIREs)*: Water, 2(6), pp.669-681. doi: 10.1002/wat2.1103.

van Thiel de Vries, J.S.M., van Gent, M.R.A., Walstra, D.J.R., and Reniers, A.J.H.M. (2008) ‘Analysis of dune erosion processes in large-scale flume experiments’, *Coastal Engineering*. Elsevier B.V., 55(12), pp. 1028–1040. doi: 10.1016/j.coastaleng.2008.04.004.

Upreti, D. *et al.* (2019) ‘A Comparison of Hybrid Machine Learning Algorithms for the Retrieval of Wheat Biophysical Variables from Sentinel-2’, *Remote Sensing,* 11(5), p. 481. doi: 10.3390/rs11050481.

Verrelst, J. *et al.* (2015) ‘Experimental Sentinel-2 LAI estimation using parametric, non-parametric and physical retrieval methods - A comparison’, *ISPRS Journal of Photogrammetry and Remote Sensing*. International Society for Photogrammetry and Remote Sensing, Inc. (ISPRS), 108, pp. 260–272. doi: 10.1016/j.isprsjprs.2015.04.013.

de Vries, M. *et al.* (2018) '*Earth Observation and the Coastal Zone: from global images to local information'*. FAST FP7 Project synthesis. GeoEcoMar, 2018. doi.org/10.5281/zenodo.1158437

Weiss, M. and Baret, F. (2016) ‘S2ToolBox Level 2 products: LAI, FAPAR, FCOVER’, *Sentinel2 ToolBox Level2 Products*. Available at: http://step.esa.int/docs/extra/ATBD_S2ToolBox_L2B_V1.1.pdf.

van Wesenbeeck, B. K. *et al.* (2017) ‘Coastal and riverine ecosystems as adaptive flood defenses under a changing climate’, *Mitigation and Adaptation Strategies for Global Change,* 22(7), pp. 1087–1094. doi: 10.1007/s11027-016-9714-z.

Williams, L., Harrison, S. and O’Hagan, A. M. (2012) ‘*The Use of Wetlands for Flood Attenuation*’, Report for An Taisce by Aquatic Services Unit, University College

Cork. Available at: https://www.yumpu.com/en/document/view/20022355/the-use-of-wetlands-for-flood-attenuation-final-report-an-taisce

Yang, S. L. *et al.* (2012) 'Wave Attenuation at a Salt Marsh Margin: A Case Study of an Exposed Coast on the Yangtze Estuary', *Estuaries and Coasts*, 35(1), pp. 169–182. doi: 10.1007/s12237-011-9424-4.

Zheng, G. and Moskal, L. M. (2009) 'Retrieving Leaf Area Index (LAI) Using Remote Sensing: Theories, Methods and Sensors', *Sensors*, 9(4), pp. 2719–2745. doi: 10.3390/s90402719.

Figures

Tables